

Article

Characteristics, Controlling Factors and Reservoir Quality Implications of Inner Fracture Zones in Buried Hills of Archean Covered Metamorphic Rock in Block 13-2, Bozhong Depression

Junjie Lu ¹, Xuanlong Shan ^{1,*}, Jian Yi ¹, Huiyong Li ², Peng Xu ², Guoli Hao ¹ , Ang Li ¹, Shuai Yin ^{3,*} , Shuyue Ren ¹, Chaoyang Liu ¹ and Yunqian Shi ¹

- ¹ College of Earth Science, Jilin University, Changchun 130061, China; jjl22@mails.jlu.edu.cn (J.L.); yijian@jlu.edu.cn (J.Y.); haoguoli@jlu.edu.cn (G.H.); liang2020@jlu.edu.cn (A.L.); syren20@mails.jlu.edu.cn (S.R.); zhaoyang18@mails.jlu.edu.cn (C.L.); shiyq20@mails.jlu.edu.cn (Y.S.)
² Tianjin Branch of China National Offshore Oil Company Ltd., Tianjin 300459, China; lih11@cnooc.com.cn (H.L.); xupeng17@cnooc.com.cn (P.X.)
³ School of Earth Science and Engineering, Xi'an Shiyou University, Xi'an 710065, China
* Correspondence: shanxl@jlu.edu.cn (X.S.); speedsys@163.com (S.Y.)

Abstract: Inner fracture zones play a decisive role in the formation of high-quality reservoirs in buried hill reservoirs in covered metamorphic rock. Based on core, sidewall core, thin section, seismic, logging and reservoir physical property data, the fracture development characteristics of the Bozhong 13-2 block buried hill reservoir are described in detail and the controlling factors and the influence on reservoir quality are discussed. The results showed: (1) three groups of tectonic fractures developed in the study area—near-EW-striking, ENE-striking and nearly N–S-striking fractures—were controlled by the early Indosinian thrusting, the late Indosinian to early Yanshanian sinistral strike-slipping and the late Yanshanian late dextral strike-slipping in the Bohai Bay Basin, respectively. The ENE- and nearly-E-W-striking fractures are the most common, and the dip angles of the fractures are mostly between 35° and 75° and thus oblique. (2) The Indosinian-early Yanshanian was the main fracture-forming period, and the dextral strike-slip action in the late Yanshanian was the key to maintaining effective fractures. Imaging logging shows that 97.87% of the fractures are effective fractures. Based on thin section observation, 14.47% of the fractures are unmodified open fractures and 80.37% of the fractures are effective fractures due to reactivation. (3) The late Yanshanian strike-slip fault transformed the deformation adjustment zone formed by the early Indosinian thrust faulting and the core of the fold structure was more conducive to fracture development. The fracture density of a single well located within the deformation adjustment zone and at the core of the fold is between 0.93–1.49 m⁻¹, the fracture density of a single well located only at the core of the fold is between 0.67–0.75 m⁻¹ and that of a single well located at the wing of the fold is between 0.35–0.59 m⁻¹. Diabase dike intrusions promoted the development of local fractures. (4) Fractures promote the migration and accumulation of oil and gas, and the fracture density in the oil layer is between 0.81–2.19 m⁻¹. That in the nonoil layer is between 0.25–1.12 m⁻¹. In addition, fractures not only provide storage space but also effectively improve the reservoir capacity of the inner fracture zones of buried hill reservoirs by concentrating dissolution.

Keywords: Bohai Bay Basin; Bozhong Depression; Archeozoic; metamorphic rock; inner curtain zone of buried hills; tectonic fractures



Citation: Lu, J.; Shan, X.; Yi, J.; Li, H.; Xu, P.; Hao, G.; Li, A.; Yin, S.; Ren, S.; Liu, C.; et al. Characteristics, Controlling Factors and Reservoir Quality Implications of Inner Fracture Zones in Buried Hills of Archean Covered Metamorphic Rock in Block 13-2, Bozhong Depression. *Energies* **2024**, *17*, 1345. <https://doi.org/10.3390/en17061345>

Academic Editor: Manoj Khandelwal

Received: 9 February 2024

Revised: 5 March 2024

Accepted: 8 March 2024

Published: 11 March 2024



Copyright: © 2024 by the authors. Licensee MDPI, Basel, Switzerland. This article is an open access article distributed under the terms and conditions of the Creative Commons Attribution (CC BY) license (<https://creativecommons.org/licenses/by/4.0/>).

1. Introduction

Buried hill is a special type of reservoir [1]. With the deepening of oil and gas exploration, many oil and gas fields with buried hill as reservoir have been found in many basins around the world such as Bach Ho oil field in the Cuu Long Basin, Vietnam [2], the buried

hill in the Bongor Basin, Chad [3,4], the La Paz-Mara gas field in Venezuela [5] and the Arysium oil and gas field in the South Turgay Basin, Kazakhstan [6].

Buried hill oil and gas reservoirs are usually located in the crystalline basement of the basin [7,8], and generally have the characteristics of large burial depth, large reservoir thickness and strong reservoir heterogeneity [1,8]. The controlling effect of fractures on basement reservoirs in basins has been widely recognized [2,3,9,10]. Metamorphic rocks have almost no primary pore space [11] and often experience multi-stage metamorphism and tectonism [7]. Fractures play a fundamental role in the formation of large-scale metamorphic buried hill reservoirs [8]. Fractures formed by tectonic activities can not only provide a channel for fluid migration, promote the migration and accumulation of oil and gas and the occurrence of corrosion, but also an important reservoir space [6,12]. Previous studies have shown that the formation of fractures is controlled by a variety of geological factors including lithology, weathering and tectonic stress [13,14]. It is generally believed that rocks rich in brittle minerals (such as feldspar and quartz) are more prone to form fractures under the same tectonic stress [14,15]. Weathering can lead to a decrease in rock density, loose texture and lower rock strength, ultimately leading to the development of fractures [1–3,14,16]. In addition, tectonic styles such as faults control the development of fractures by influencing local tectonic stress, and the degree of fracture development is often negatively correlated with the distance from the fault surface [17]. The main controlling factors of fracture development in different types of buried hills in different basins are quite different.

Bohai Bay Basin is an important oil-bearing basin in China [18] (Figure 1b) and Archean metamorphic buried hills are important areas for deep oil and gas exploration there [19]. The Bohai Bay Basin was transformed by multiple tectonic activities, especially the Indosinian and Yanshanian movements, which formed many various types of buried hills within the basement [8,20,21]. Buried hill oil and gas reservoirs with Archean metamorphic rocks were discovered in the Bohai Bay Basin as early as the 1970s [22]. In recent years, the Jinzhou 25-1 south metamorphic buried hill gas field [23] and the Chengbei area of the Jiyang Depression have been discovered [24] (Figure 1b). The discovery of the Bozhong 19-6 Archean metamorphic buried hill condensate gas field in 2019 opened a new avenue for the exploration and development of basement-exposed buried hill hydrocarbon reservoirs in the Bohai Bay Basin [25]. The discovery of a 100-million-ton Archean metamorphic buried hill oil and gas field in the Bozhong 13-2 block in 2021 further proves the exploration potential of deep Archean metamorphic buried hills in the Bohai Bay Basin [26] (Figure 1b). The Bozhong 19-6 Archean exposed buried hills are in direct contact with Cenozoic sedimentary strata, the weathering time is long and the weathered crust is relatively developed, forming a two-layer reservoir development model composed of a weathered crust reservoir and an inner reservoir [27]. Unlike the Bozhong 19-6 buried hill reservoir, the Bozhong 13-2 buried hill reservoir is overlain by dense Mesozoic strata and was not extensively weathered during the late Yanshanian period [27]. Only a very thin weathered crust developed on the top of the buried hill, and the formation of reservoir is more significantly influenced by tectonic activities [26,27]. Therefore, finding the inner fracture zone is key to the exploration of covered buried hill reservoirs.

For the BZ19-6 exposed Archean metamorphic buried hill, several scholars have explored the distribution and genesis of fractures from the perspective of the large-scale structural background [15,28] but ignored the control of the local stress field on fracture development. Research has shown that it is difficult to determine the distribution and development evolution of regional fractures from a large-scale structural background. Detailed studies of the relationship between the distribution and development evolution of fractures in buried hills of metamorphic rock are still limited, and there is a lack of systematic discussion. The Bozhong 13-2 oil and gas field studied in this research is located southwest of the Bozhong Sag, and the southern part is described as the Bozhong 19-6 gas field (Figure 1b). This study takes the Bozhong 13-2 Archean metamorphic buried hill in the Bozhong Sag, Bohai Bay Basin, as the main research object. We make full

use of the core, sidewall core, thin section, SEM, physical property, imaging logging, seismic and fluid inclusion data of six typical drilling wells that encountered the Archean metamorphic buried hill in the study area to study the reservoir fractures in this stratum. The characteristics of the fractures are described in detail from different perspectives, the enrichment effect of local stress field on fractures is emphatically discussed and the influence of the fractures on the reservoir quality is clarified. This work is highly important for the further exploration and development of the study area and provides a reference for the exploration of basement metamorphic rock with reservoirs with inner fracture zones in other basins worldwide.

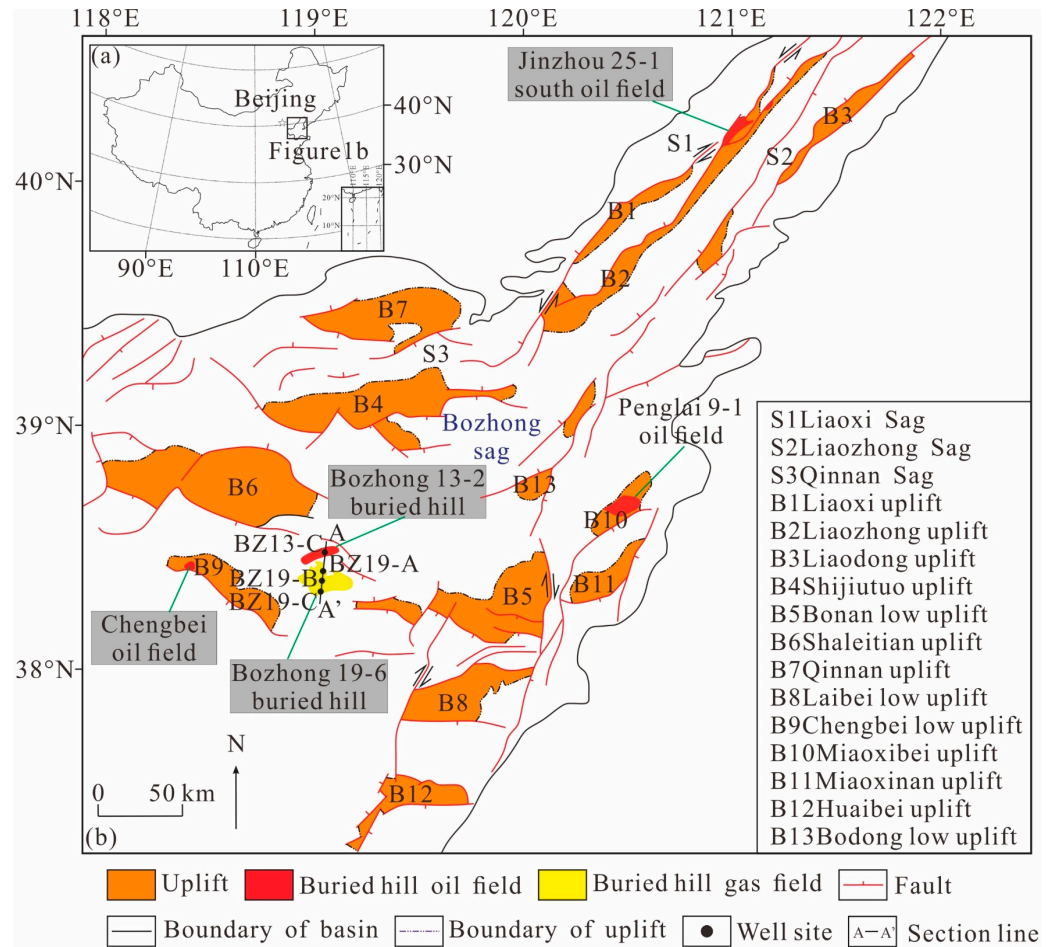


Figure 1. Structural outline map and comprehensive stratigraphic column diagram of buried hills in Bohai Bay Basin. (a) Location of Bohai Bay Basin; (b) structural outline map of Bohai Bay Basin, modified after Yi et al. (2022) [27].

2. Geological Setting

The Bohai Bay Basin is located in the eastern North China Craton, covers an area of 20×10^4 km² and is a typical Meso-Cenozoic continental oil-bearing rift basin [29]. The area of oil-bearing strata in the Bohai Bay is 4.4×10^4 km², which is mainly composed of the Bozhong Sag, Qinnan Sag, Liaozhong Sag, Shaliangtian uplift, Bonan Low uplift, Qinnan uplift and other secondary structural units. Located in the central and eastern parts of the Bohai Bay Basin, the Bozhong Sag is the largest oil-rich sag in the Bohai Bay Basin, with an area of approximately 1×10^4 km² bounded by the Bodong low uplift to the east, the Shaleitian uplift to the west, the Shijiutuo uplift to the north, and the Bonan low uplift to the south [27] (Figure 1b). The Bozhong Sag experienced vertical uplift of the basement before the Indosinian period, and the basic outline of the buried hill in the Archean strata was formed by early Indosinian thrust compression [7,8,12,20].

The Bozhong 13-2 oil and gas field has been drilled to reveal that the strata from bottom to top are Archean strata, the Mesozoic strata, the Palaeogene Shahejie and Dongying Formations, the Neogene Guantao and Minghuazhen Formations and the Quaternary Pingyuan Formation (Figure 2). The main strata in this study are Archean basement, and drilling data show that most metamorphic rocks have experienced intrusion [7,12]. The basement buried hill has undergone complex tectonic events—the Indosinian, Yanshanian and Himalayan tectonic movements [7] (Figure 2). Among them, the Indosinian and Yanshanian tectonic movements largely controlled the Bozhong structural belt [30,31]. Under the influence of strong Indosinian thrusts (Triassic–early Jurassic) [27], the top Palaeozoic strata of the Bozhong 13-2 buried hill were completely denuded [32]. The middle Yanshanian (late Jurassic–Early Cretaceous) underwent regional extension, with the Bozhong 13-2 oil and gas field buried by Mesozoic strata [33]. In the late Yanshanian (late Cretaceous), reverse faulting and slipping occurred again [20,33]. However, the denudation of the top of the Bozhong 13-2 buried hill was weak and the top Mesozoic strata were retained, forming a hill buried by the overlying Mesozoic strata [27]. The main lithology of the Archean buried hill is granitic gneiss, and the buried hill is directly overlain by dense and thick Mesozoic tuffaceous conglomerate and sediment, serving as a good caprock for the corresponding buried hill reservoir [26,28,30,33] (Figure 2).

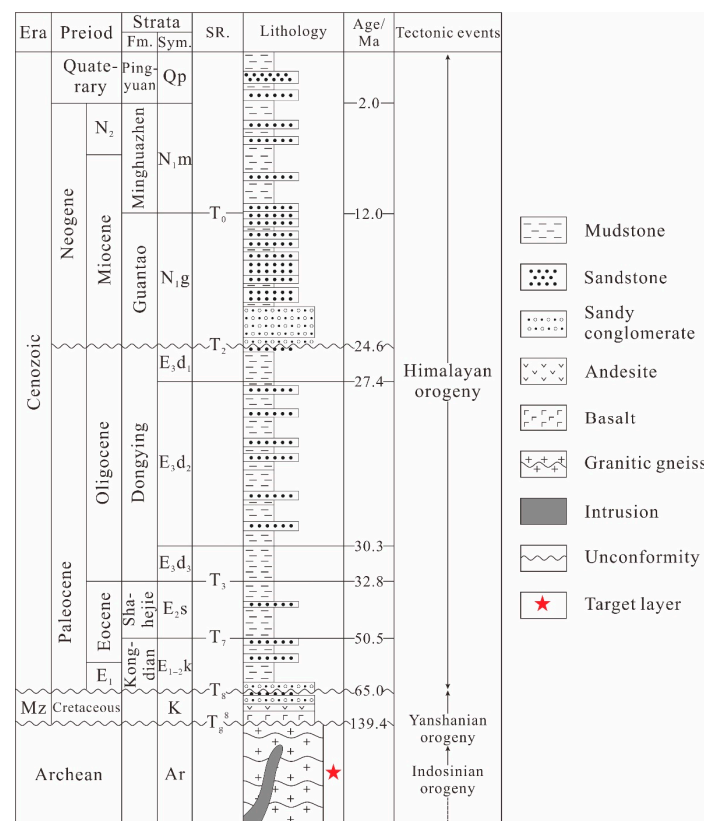


Figure 2. Lithology comprehensive column diagram of Bozhong 13-2 block, modified after Li et al. (2021) [26]. Fm. = formation; Sym. = symbol; SR. = seismic reference; Mz = Mesozoic; E₁ = Paleocene; N₂ = Pliocene.

3. Materials and Methods

Samples from core with a total length of 2.9 m and 97 sidewall cores were collected from 6 wells and observed to determine the lithology and fractures.

A total of 179 ordinary and casting thin sections were collected and observed to identify the microscopic characteristics of fractures, filling and dissolution along microfractures. Casting thin sections (30 μm in thickness) with blue dye resin were used to analyze the

effective fractures and pores [34]. Thin sections were analyzed using a Zeiss Axio Scope A1 polarized optical microscope with a ICCS optical system.

The clay minerals and microscopic characteristics of fractures were observed by scanning electron microscopy (SEM). In the SEM sample preparation process, the sample was first cut into blocks with a width of about 8 mm, and then mechanically polished with sandpaper with precision (roughness) of 9.0, 2.0 and 0.5 μm , respectively. The sandpaper used for grinding should be from coarse to fine, and the same was repeated 20 times to ensure the sample surface was smooth. Finally, argon ion polishing was performed [35]. In the process of argon ion polishing, the current was 2.1 mA and the voltage was 5.5 kV. The voltage was switched to 5.0 kV and 2.0 mA every 30 min, and the sample preparation was repeated 4 times. The surface of the sample was treated with carbon spray to form a conductive film. 42 samples were observed by SEM using a Zeiss Merlin Compact. A KV voltage of 20 was used to obtain electron microscope images. The experimental magnification is between 200–8000 times.

We observed the fluorescence characteristics of 122 fluid inclusion images of 8 samples and analyzed the occurrence location and characteristics of oil and gas. The equipment used was Leica DM4500 fluorescence microscope.

Imaging logs were collected from the China National Offshore Oil Corporation Limited, Tianjin Branch, Tianjin, including 6 wells with a total length of 1918 m. Schlumberger Techlog 2015.3 software was used to identify different types of fractures (conductive fractures, resistive fractures and induced fractures) and calculate the fracture parameters (strike, dip angle and linear density of fractures).

A 3D seismic dataset was obtained from the China National Offshore Oil Corporation Limited, Tianjin Branch, Tianjin, which covers approximately 1824 km² of the study area. The data are relatively good, with a 25 m \times 25 m bin, a 2 ms vertical sampling rate and a 35 Hz dominant frequency.

A total of 63 reservoir analyses data sets including porosity and permeability were collected from the China National Offshore Oil Corporation Limited Tianjin Branch (CNOOC) to determine the relationships between physical properties of the rocks and fractures. The process of this study is shown in Figure 3.

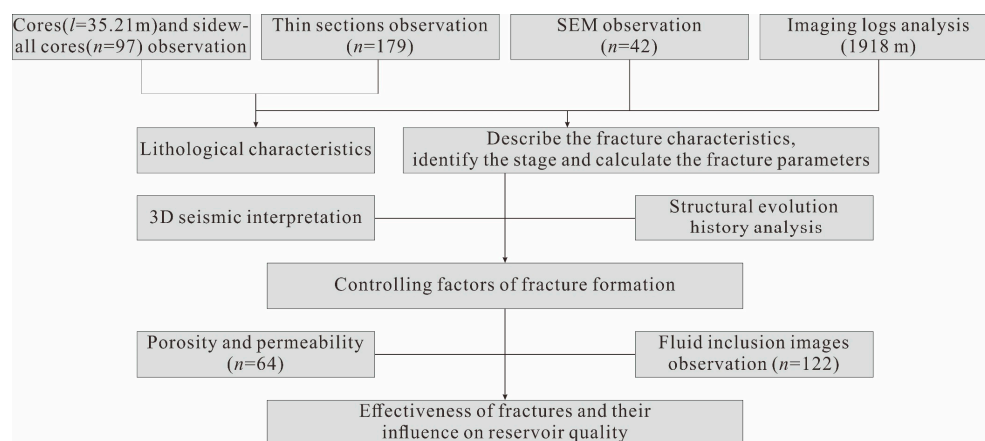


Figure 3. Flow chart of fracture research.

4. Results

4.1. Lithological Characteristics

The main lithology of the Archaean buried hill is metamorphic rock, which can be further divided into granitic gneiss and cataclastic rock [7,8]. Granitic gneiss is the most widely distributed rock and is the main object of study. Within these metamorphic rocks, intersections by intrusive dikes are found [7,12].

The granitic gneiss is the product of regional metamorphism. The granite gneiss is light-grey/white in the core, with local dark bands. It has gneissic texture (Figure 4a,e).

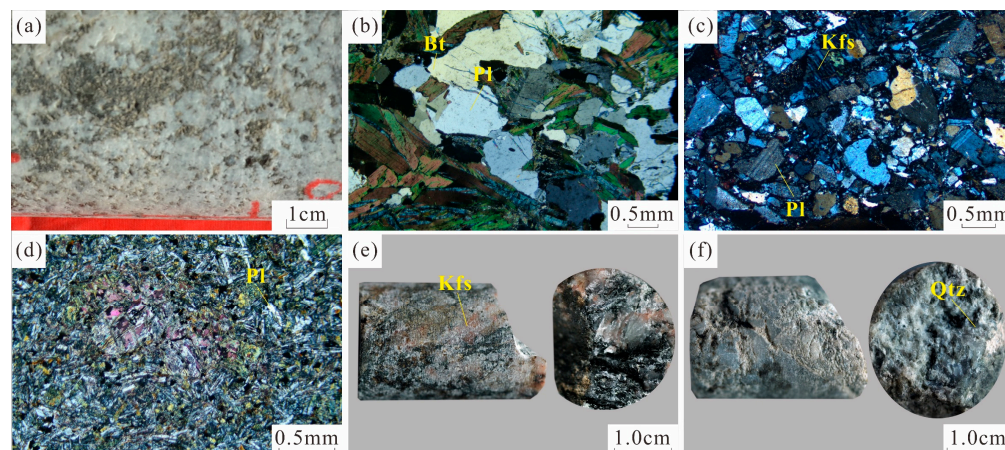


Figure 4. Typical lithology in inner zone of Archaean buried hill in Bozhong 13-2 block. (a) Granitic gneiss, core, BZ13-C, 4716.66 m; (b) granitic gneiss, thin section, BZ13-B, 5025.00 m; (c) cataclastic rock, thin section, BZ13-D, 5090.00 m; (d) diabase, thin section, BZ13-B, 5040.00 m; (e) granitic gneiss, sidewall core, BZ13-B, 5025.00 m; (f) cataclastic rock, sidewall core, BZ13-B, 5129.00 m. Bt = biotite, Qtz = quartz, Kfs = K-feldspar, Pl = plagioclase.

The granite-gneiss is mainly composed of plagioclase, quartz, alkaline feldspar and a small amount of biotite, the contents of which are about 30–40 vol%, 20–30 vol%, 10–20 vol%, 3–5 vol%, respectively, and the content of light-colored minerals is high. Biotite presents a directional discontinuous distribution (Figure 4b).

Cataclastic rock is the product of dynamic metamorphism, which is formed when primary rock is broken under strong stress [6]. The core is variegated color and has a cataclastic texture (Figure 4f). The mineral particles in the thin sections are seriously fragmented, and there are fine mineral fragments between minerals particles (Figure 4c). Cataclastic rocks are mainly distributed near faults.

Thin layer diabase intrusion dikes can be found in metamorphic rock mass. It can be observed in the thin section that the diabase is mainly composed of plagioclase phenocrysts. The gap between plagioclase phenocrysts is filled with pyroxene particles and has a typical diabase texture. The rock as a whole is seriously chlorinated (Figure 4d). The thickness of diabase dikes drilled in the study area is usually less than 20–25 m, and the intrusion time is about 117 M [7].

4.2. Characteristics and Stages of Tectonic Fractures

Fractures are discontinuities that form in rocks due to brittle and semi-brittle deformation [36]. The results of sidewall core and thin section observations show that tectonic fractures and nontectonic fractures developed in the inner fracture zone of the studied buried hill, in which tectonic fractures are dominant and nontectonic fractures are rarely observed. Therefore, this paper focuses on the tectonic fractures, which are structures that occur due to discontinuous displacement during tectonic activity between two surfaces or within a region [36–38].

4.2.1. Fracture Characteristics and Phase Identification via Thin Section and SEM

Thin section analysis is an important means to observe fracture characteristics [34]. We can identify and describe the fracture stages and properties by observing the microscopic characteristics of fractures in thin section under a microscope. A group of tectonic fractures with the same or similar angles are generated in the same phase of structural movement, and the relative number of fractures in different groups is often related to the fracture-forming capacity of the corresponding phase of tectonic activity. Therefore, the fracture stages can be identified by the mutual cutting relationship between the fractures and fracture angles [34]. At least three stages of tectonic fracturing were identified at the microscopic scale through

the observation of many thin sections, and in the following Figure 5 the stages are indicated by color: the number of fractures indicated by the yellow lines is significantly greater than that indicated by the green and red lines (Figure 5a–c), indicating that the corresponding tectonic activity had the greatest fracture formation capacity. Earlier fractures are often cut by later fractures, and the earlier fractures can become offset. We observe that fractures indicated by yellow lines are often offset by fractures indicated by green and yellow lines (Figure 5b), while fractures indicated by green lines are offset by fractures indicated by yellow lines (Figure 5c). Therefore, it was concluded that the fractures that formed in the first phase are marked by yellow lines, the fractures that formed in the second phase are marked by green lines, and the fractures that formed in the third phase are marked by red lines.

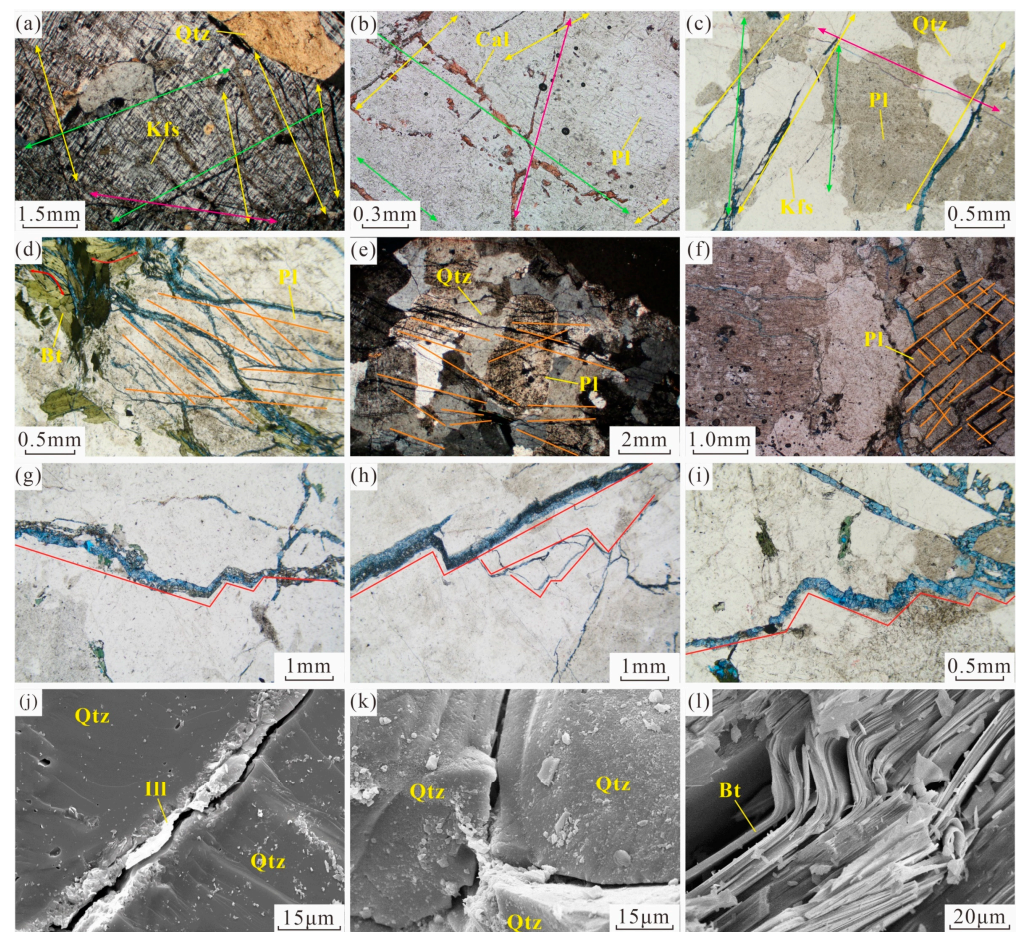


Figure 5. Microscopic characteristics of fractures in the inner zone of Archaeon buried hill in Bozhong 13-2 block ((a–i) are thin section images, (j–l) are SEM images). (a) Three groups of oblique fractures developed in the microcline, BZ13-A, 4464.00 m; (b) three groups of oblique fractures developed in the feldspar, BZ13-D, 5082.50 m; (c) three groups of oblique fractures developed in the feldspar and quartz, BZ13-B, 4946.00 m; (d) tectonic stress produces plastic deformation in biotite, brittle deformation in feldspar, BZ13-B, 5025.00 m; (e) network tectonic fractures in feldspar and quartz, BZ13-A, 4410.00 m; (f) two groups of nearly right angle dense network tectonic fractures in feldspar, BZ13-D, 4925.00 m; (g) group of stepped shear joint, BZ13-B, 4655.00 m; (h) multiple groups of stepped shear joints, BZ13-B, 4720.00 m; (i) group of stepped shear joint, BZ13-B, 4963.00 m; (j) fracture in quartz crystals, slightly filled with filamentous illite, BZ13-B, 4729.00 m; (k) fracture between quartz crystals, BZ13-C, 4628.00 m; (l) sheet biotite is compressed by tectonic stress and deforms, BZ13-B, 4717.76 m. Qtz = quartz, Kfs = K-feldspar, Cal = calcite, Pl = plagioclase, Bt = biotite, Ill = illite.

Tectonic fractures are produced in different forms in minerals with different crystallization habits. The tectonic fractures in brittle minerals such as quartz and feldspar, both granular and platy, tend to be relatively straight, extend far and have good connectivity and thus were the main sites of fracture development (Figure 5j,k). Since cleavage is more common in feldspar crystals than in quartz crystals, fracture networks formed more often in the feldspar crystals, which greatly promoted the migration and storage of oil and gas (Figure 5e,f). The tectonic fractures identified in the sheet minerals such as biotite tend to curve and not extend very far, which is caused by the sheet crystal structure of biotite, as stress release tends to bend sheet mica rather than cause dislocation (Figure 5l). The stepped fractures that formed in the brittle minerals show that the fractures were mainly formed by compressive stress (Figure 5g-i).

The microscopic characteristics of the fractures also reveal that most of the fractures are open and have good oil and gas seepage and storage capacity, but they exhibit obvious reactivation characteristics. Figure 5j shows that the fractures were filled with minerals such as illite after they formed but that new tectonic fractures reactivated the edges of the fractures, which are characterized by “seam-edge fractures” [15]. Such reactivation is extremely common.

4.2.2. Fracture Characterization and Phase Identification via FMI Logging

In areas without cores, high-resolution FMI logging, which provides structural information around the borehole, is an effective fracture characterization method [9,39]. High-resolution FMI logging can be used to determine the filling status (open, filled and partially filled) and orientation information (strike and dip angle) of fractures [40]. We can identify different natural fractures (conductive fractures and resistive fractures) and induced fractures by FMI logging. In the process of drilling, due to the intrusion of water-based mud with high conductivity, open fractures (namely conductive fractures) are shown as black continuous sine waves on FMI logs (Figure 6a) [34]. When fractures are filled with high-resistance carbonate or siliceous minerals, high-resistivity fractures (ineffective fractures) are detected, which appear as bright continuous sine waves in FMI logs (Figure 6b) [34]. The induced fractures are shown as a set of feathered or en echelon fractures parallel to each other and 180° symmetric at high angles (Figure 6c).

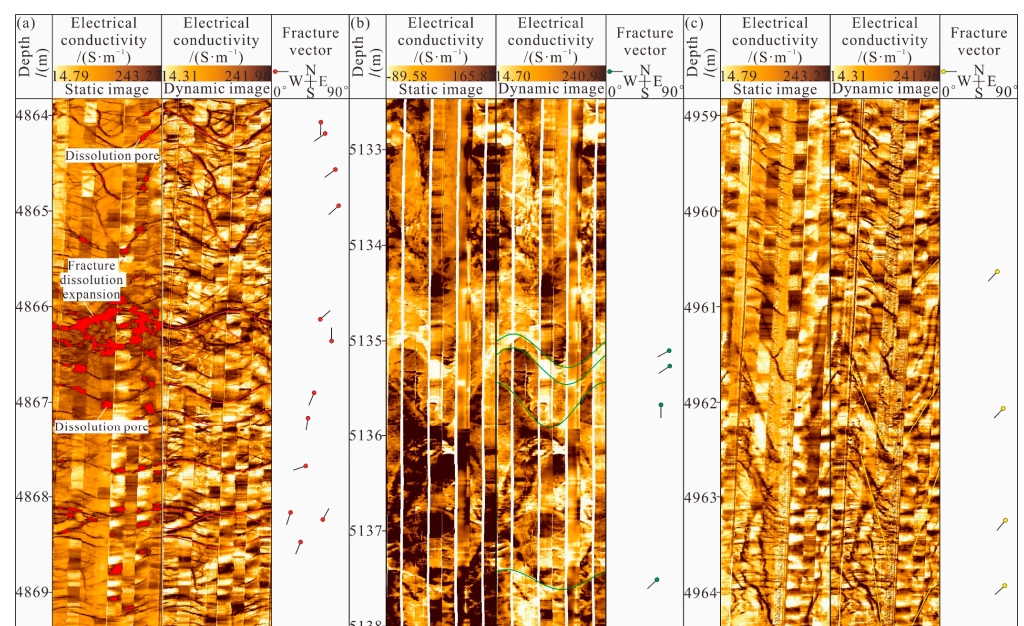


Figure 6. FMI characteristics of conductive fracture, resistive fracture and induced fracture in the inner zone of Archaean buried hill in Bozhong 13-2 block. (a) Characteristics of conductive fractures, (b) characteristics of resistive fractures, (c) characteristics of induced fractures.

According to the interpretation results of the imaging log data, three groups of dominant natural tectonic fractures were identified overall: ENE-trending, nearly E-W-trending and nearly N-S-trending fractures (Figure 7a). Compared to the N-S trending fractures, there are many more ENE-trending fractures and nearly E-W-trending fractures, reflecting strong tectonic activity during the formation of these two groups of natural tectonic fractures. The single-well tectonic fracture strike is obviously consistent with the fracture strike near the well location (Figure 7c), indicating that the formation of tectonic fractures was controlled by both tectonic movement and faulting. The fracture inclination angles are concentrated between 35° and 75° , and these fractures are generally oblique (Figure 7b).

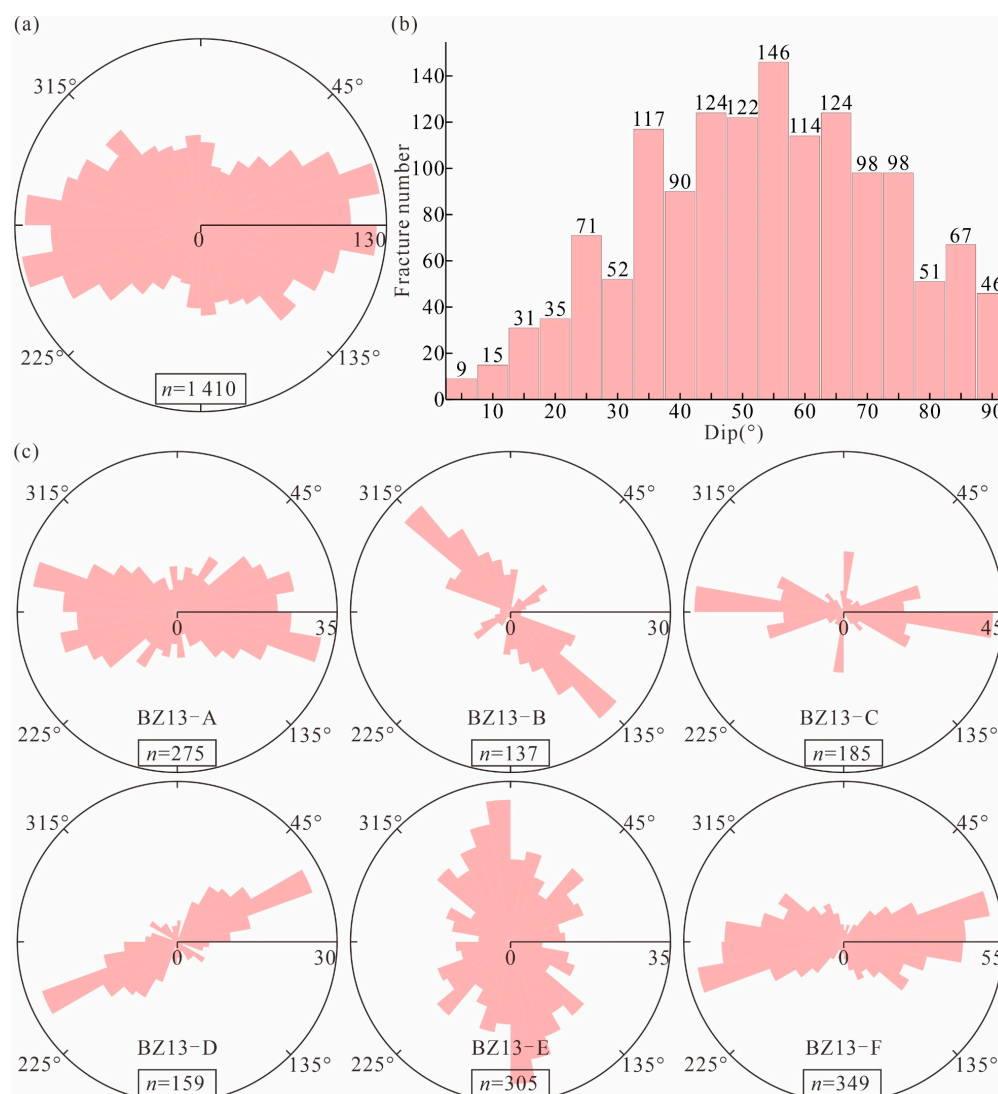


Figure 7. Characteristics of natural tectonic fracture strike and dip angle in the inner zone of Archaean buried hill in Bozhong 13-2 block. (a) Orientations of tectonic fractures; (b) dip angle of tectonic fractures; (c) orientations of single well tectonic fractures.

The orientation of induced fractures reflects the current stress field orientation in the study area. Analysis of 153 induced fractures in 6 wells in the BZ13-2 block reveals that the induced fractures strike NW (Figure 8a). The induced fracture trend of the well BZ13-E shows that the current stress field at the well location is most compressive nearly E-W, while the tectonic fracture trend is mainly nearly N-S, which may lead to the closure of the fractures. In addition, the current stress field indicated by the induced fractures in other wells is consistent with the strike of the tectonic fractures, which indicates that the

structural fractures in most wells are effectively opened (Figure 8c). The induced joint inclination angles are mainly 45–80°, and these fractures are generally oblique (Figure 8b).

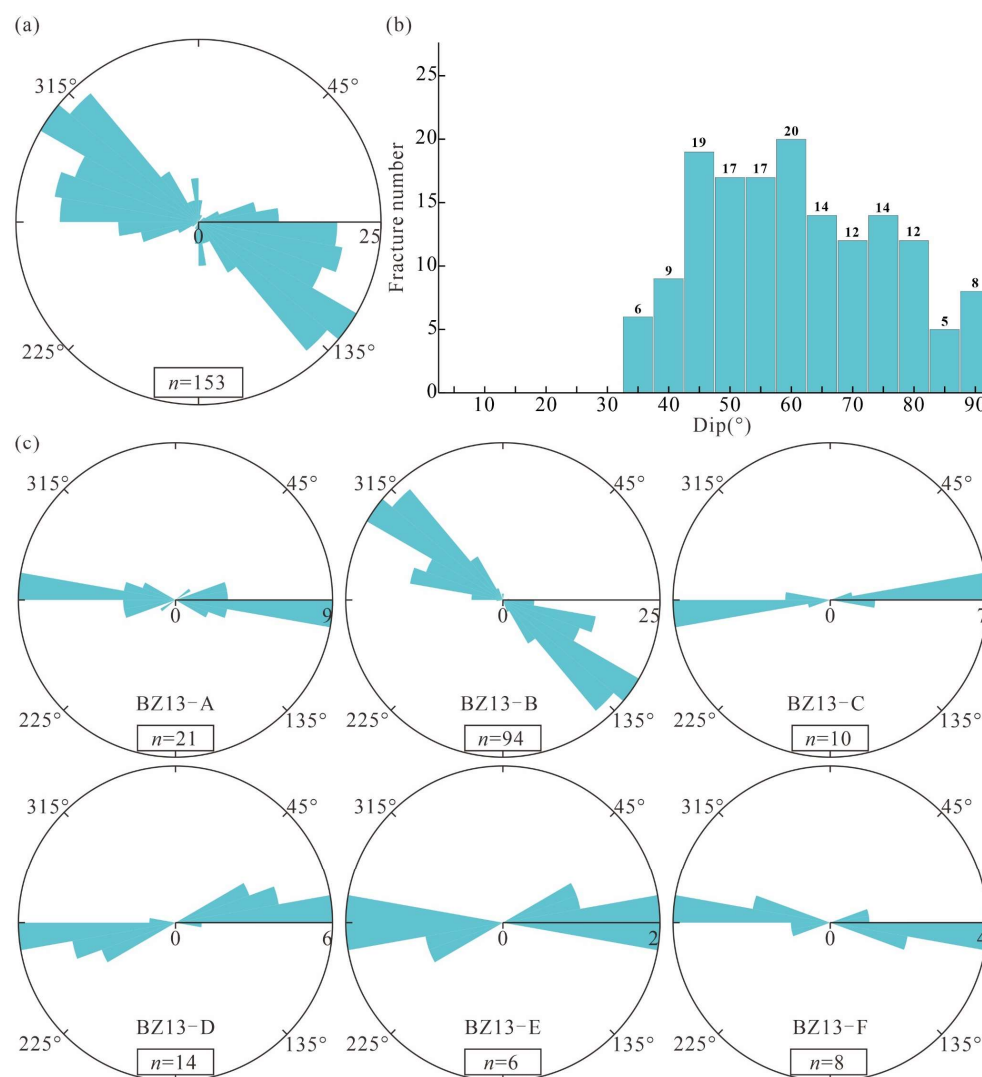


Figure 8. Characteristics of borehole induced fracture strike and dip angle in the inner zone of Archaean buried hill in Bozhong 13-2 block. (a) Orientations of induced fractures; (b) dip angle of induced fractures; (c) orientations of single well induced fractures.

The fracture linear density refers to the ratio between the number of fractures observed within a given length [41]. In quantitative studies of tectonic fractures, fracture linear density is commonly used to characterize the degree of fracture development in a formation. We calculated the fracture density in the inner fracture zone encountered in each well in the study area. The results show that the fracture linear density of the inner fracture zone varies greatly among the different wells, ranging from 0.22 to 1.49 m^{-1} . Among them, the fracture linear densities of the BZ13-B, BZ13-A and BZ13-F wells are relatively large, while the fracture linear densities of the BZ13-D and BZ13-E wells are lower than 0.6 m^{-1} , which is relatively small (Figure 9a).

According to the structure of the underground rock layer shown by static and dynamic FMI logging images, the fracture state of the inner fracture zone under the weathered crust of the buried hill in the study area was observed. A total of 1410 natural fractures were identified by statistically analyzing 1918 m of FMI logging images in the study area. The open effective fractures and filled ineffective fractures accounted for 97.87% and 2.13%,

respectively (Figure 9b), indicating that most of the fractures in the study area were still open and could serve as good reservoir spaces and drainage pathways.

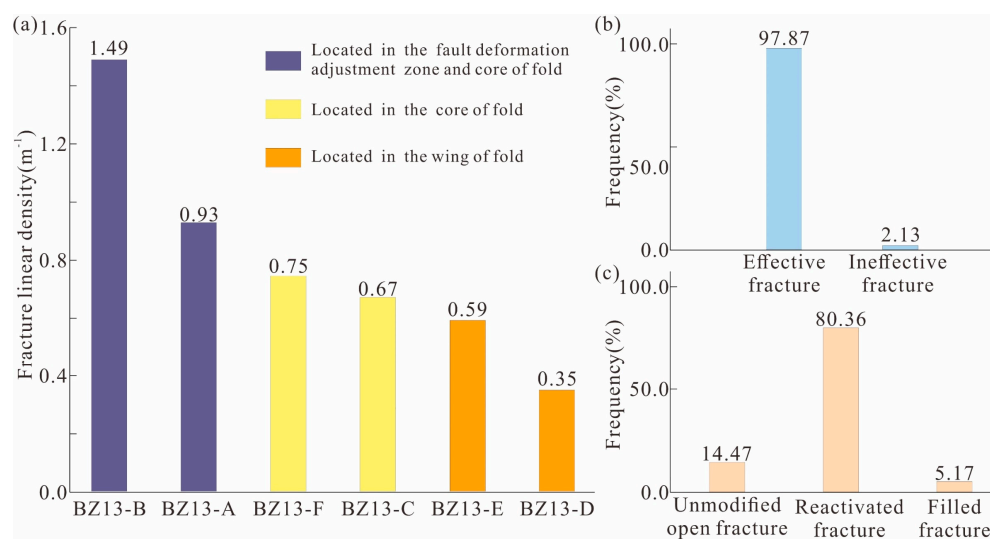


Figure 9. Distribution and state of tectonic fractures. (a) Comparison of fracture linear density in different wells; (b) fracture state statistics based on FMI logging; (c) fracture state statistics based on thin section.

According to the statistics on the reactivation of 387 fractures in 202 thin sections, there are only 56 unmodified open fractures, accounting for 14.47%; 311 fractures were reactivated after filling, accounting for 80.36%; 94.83% of the total are effective fractures; and 20 are fully filled fractures, contributing to the 5.17% ineffective fractures (Figure 9c), indicating that reactivation after fracture formation plays a crucial role in the effectiveness of the current fractures.

4.3. Petrophysical Data

In this study, the porosity and permeability test data of 64 samples were collected, including 14 cataclastic samples, 38 granitic gneiss samples and 12 diabase samples. The porosity of the cataclastic samples ranged from 1.09% to 4.01% with an average value of 2.38%, and the permeability ranged from 0.015 mD to 3.628 mD with an average value of 0.532 mD. The porosity of the granitic gneiss samples ranged from 0.92% to 10.08% with an average value of 3.73%, and the permeability ranged from 0.001 mD to 0.134 mD with an average value of 0.035 mD. The porosity of the diabase samples ranged from 2.07% to 10.04% with an average value of 4.95%, and the permeability ranged from 0.002 mD to 0.077 mD with an average value of 0.033 mD. This shows that cataclastic rock has a higher permeability while diabase has a higher porosity.

4.4. Seismic Profile

In this study, we chose two representative seismic profiles (see location in Figures 1b and 10a) to illustrate the strata contracting relationship and the structural position of each well in the study area. Section A-A' shows the difference between Bozhong 13-2 block and Bozhong 19-6 block in stratigraphic and structural position. The Mesozoic strata are overlying the Archean basement in Bozhong 13-2 block, while the Cenozoic strata are overlying the Archean basement in Bozhong 19-6 block. The basement reservoirs in Bozhong 13-2 block are less affected by weathering than those in Bozhong 19-6 block [27] Bozhong 13-2 block is in the front of nappe body, while Bozhong 19-6 block is in the center of nappe body (Figure 11a,b). Profile B-B' shows the different positions of single wells in the fold structure in Bozhong 13-2 block. BZ13-A, B, C and F wells are located in the core of the fold, while BZ13-D and E wells are located in the wing of the fold (Figure 11c,d).

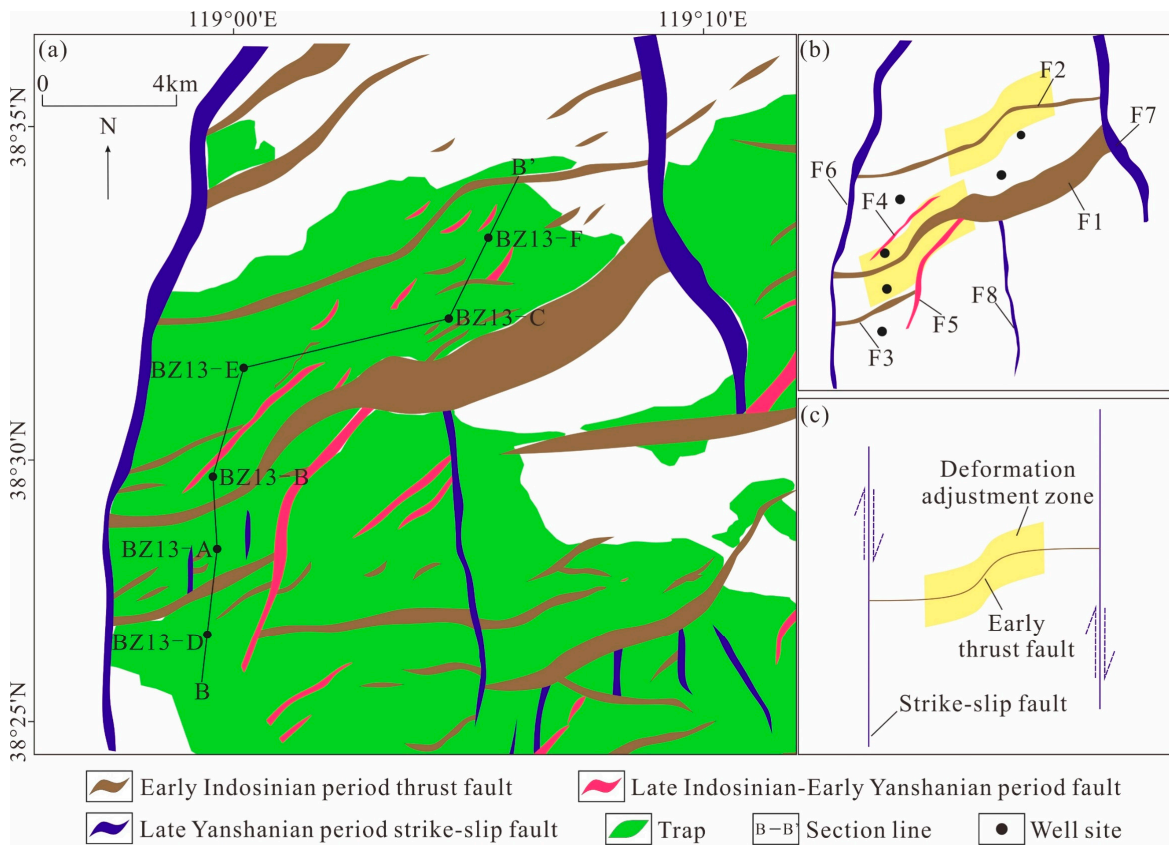


Figure 10. Fault distribution map of Bozhong 13-2 block. (a) Fault distribution map of Bozhong 13-2 block; (b) map of major faults; (c) theoretical diagram of fault deformation adjustment zone.

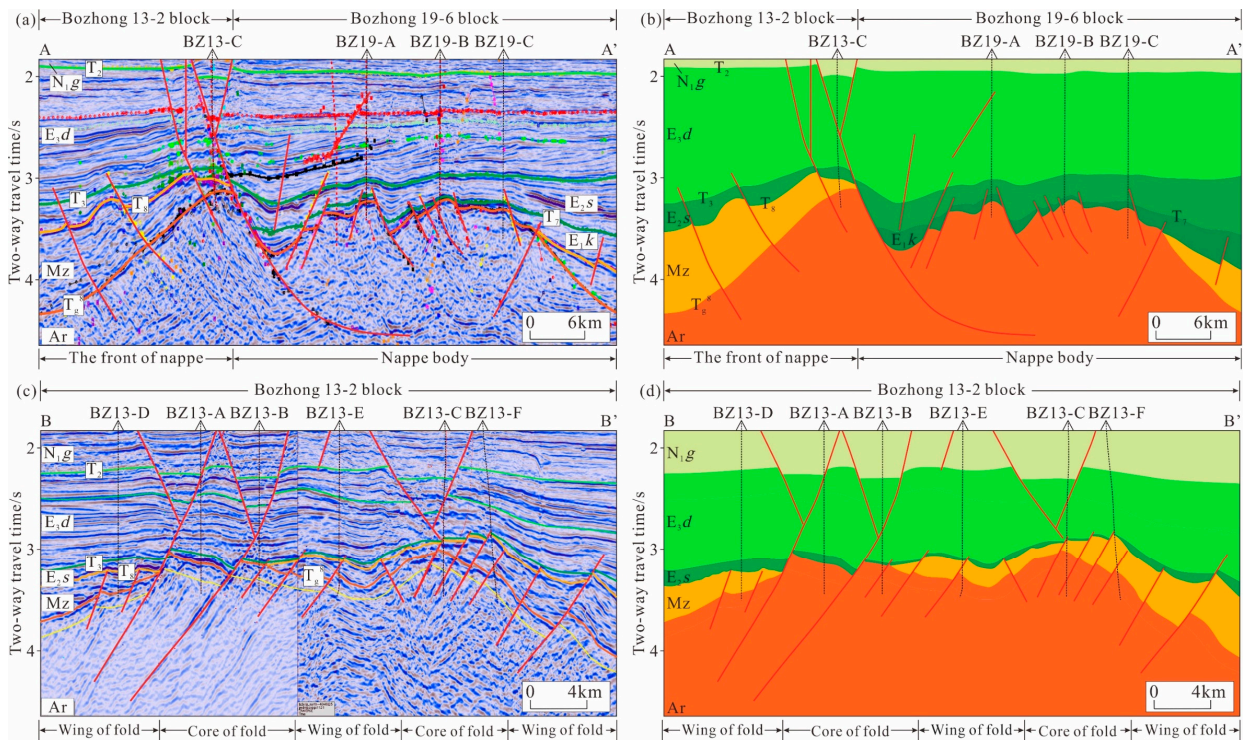


Figure 11. (a,b) Profiles of Bozhong 19-6 and Bozhong 13-2 tectonic area in Bozhong Depression, Bohai Bay Basin (for the location of the section, see (Figure 1b)); (c,d) profile of drilling position and structural position in area Bozhong 13-2 (for the location of the section, see Figure 10a).

5. Discussion

5.1. Factors Controlling the Formation of Fractures in the Inner Fracture Zone

The development and distribution of tectonic fractures are controlled by many factors, which can be divided into structural factors and nonstructural factors [13,42]. Tectonic factors are the external causes that lead to rock fracturing and faulting and are related to the regional or local stress field. The nonstructural factors affecting the development and distribution of tectonic fractures include lithology, mineral composition, weathering and other external factors [42]. The inner fracture zone of the Archaean buried hill in the Bozhong 13-2 block has a relatively simple lithology—mainly granite (granite-gneiss and granitization granite)—generally with a low content of mafic minerals [43]. Structural factors are the main factors affecting the differential distribution of fractures in the inner fracture zone [7,8,12,43].

5.1.1. Three-Stage Tectonic Movement Is the Foundation of Fracture Development

Tectonic fractures are the main reservoir space of metamorphic buried hills. Thus, tectonic movements play an important role in controlling the formation of fractures [15,19,25,26]. The basement of the Bohai Bay Basin is part of the North China Block, and the characteristics of the basin structure and sedimentary distribution indicate that thrust/compressional nappe structures and strike-slip structures are the main structural types in the Bohai Bay Basin [20,43–45]. Previous studies have confirmed that the Archaean metamorphic in the Bohai Bay Basin experienced extremely complex tectonic movements and geological processes after their formation. Since the formation of the Archaean buried hill, especially the destruction of the North China Craton since the Mesozoic era, many tectonic fractures have formed during the processes of orogeny and basin formation, including the thrust extrusion in the early Indosinian, the late Indosinian to early Yanshanian sinistral strike-slip thrusting and the late Yanshanian dextral strike-slipping [15,28,44,45].

In the early Indosinian period, the subduction of the South China plate beneath the North China plate resulted in a regional compressive stress field from the south to the north [20,31,32,45]. During this time, a series of thrust faults formed from south to north, and faults were mainly distributed nearly E-W [15,44]. These faults controlled the formation of nearly E-W-trending fractures. From the late Indosinian period to the early Yanshanian period, the Palaeo-Pacific plate subducted under the Eurasian plate at a high angle, and under the influence of the Tanlu fault system, the whole Bohai Bay Basin was in a sinistral compressive and torsional stress field under the action of sinistral shear stress, while the study area was in a NW–SE compressive stress field [20,31,32,45]. Therefore, NE-trending thrust faults developed on the basis of the nearly E-W-trending faults in the early Indosinian period [44]. The associated fractures strike ENE. The subduction of the Palaeo-Pacific plate beneath the Eurasian plate in the middle Yanshanian period caused upwelling of the mantle diapir, the thrust faults in the basin generally reversed and the stress mechanism changed from a collisional subduction system to an extensional system [20,31,32,43–45]. Under this tectonic background, the fractures that provided the main reservoir space for the oil and gas may have closed or filled during this period [15,23,28]. In the late Yanshanian period, the Palaeo-Pacific plate subducted under the Eurasian plate at a low angle nearly from the east to the west, and the Bohai Bay Basin experienced a change from sinistral strike-slip shear to dextral strike-slip shear, forming a series of NNE-trending strike-slip faults controlled by the Tanlu fault in the east and the Shaleitian uplift in the west [32,45]. According to this stress field model, several nearly N-S-trending tectonic fractures are generated in the study area, and this inheritance promotes further development and reactivation of these fractures. The strike-slip faults are generally large in scale and have a great influence on the depth, so this period was the key period for ensuring the effectiveness of basement fractures [23,28]. After entering the Cenozoic era, the Bohai Bay Basin as a whole was under a dextral tensile tectonic regime and the faults generated during this stage were generally shallow and small, mostly existing during the Cenozoic Epoch [20,44,45]. Furthermore, these faults had little effect on the transformation of Archaean metamorphic buried hills

and did not contribute significantly to the generation of fractures but played a certain role in maintaining the effectiveness of fractures and optimizing and improving oil storage structures [7,23,28,45].

Studies have shown that massive fractures are more likely to develop in a compressive stress field than in a tensile stress field [15]. The strong thrusting and dextral strike-slip/thrusting of the Indosinian–Yanshanian period led to the uplift of the Bozhong 13-2 block, which controlled the distribution of Palaeozoic strata and was also the formation period of massive basement fractures, laying the foundation for fracture reactivation during later tectonic movements [12,15,28,29,43].

5.1.2. Tectonic Location Determines the Degree of Fracture Enrichment

Some natural fractures are the product of tectonic activity, and their formation is mainly related to faulting and folding [46–49]. The degree of fracture development is strongly correlated with the degree of stress concentration and deformation. The area where the orientation of the strata changes significantly (including the intersection of the fault and the core of the anticline) has a high stress concentration, high deformation degree and high fracture density [46,47]. As mentioned above, the Bohai Bay Basin formed the present tectonic pattern during multistage tectonic movement from the Indosinian to the Himalayan period. Due to the Indosinian thrust nappe, the Bozhong 19-6 block is in the main area of the nappe body, and the Bozhong 13-2 block is in the front of the entire nappe structure (Figure 11a,b). A series of early Indosinian NNE-trending thrust faults, such as F2 and F3, and a small number of late Indosinian and early Yanshanian NE-trending thrust faults developed from north to south. The F6 and F7 late Yanshanian nearly N-S-trending strike-slip faults are confined to the eastern and western study area, respectively, and the F8 late Yanshanian strike-slip faults develop in the centre (Figure 10a,b). In terms of fault morphology, the early Indosinian thrust faults constrained by late Yanshanian strike-slip faults at both ends exhibit an “S” shape, while the normal early Indosinian thrust faults exhibit a “curved” shape (Figure 10b). The “S”-shaped thrust fault was the result of modification and adjustment under the influence of the dextral strike-slip stress field in the late Yanshanian period (Figure 10c), its centre was a two-stage tectonic deformation adjustment zone and the effect of tectonic deformation adjustment on both the ends and sides of this fault was weakened. The relationship between the fracture density and structural location reveals that fractures are more developed in the structural deformation adjustment zone where the linear density of fractures is usually greater than 0.93 m^{-1} (Figure 9a).

The seismic profile shows that the Bozhong 13-2 block was affected by the compressive stress field from the Indosinian to Yanshanian and that several anticlinal structures formed inside the tectonic area (Figure 11c,d). Previous studies have shown that the stress in the core is more concentrated and the deformation degree is greater than that in the wing, so the core of the fold is more likely to develop structural fractures [50–53]. According to the shape of the fold on the seismic profile, the BZ13-A, BZ13-B, BZ13-2-C and BZ13-F wells are in the core of the fold, while the BZ13-D and BZ13-E wells are in the wing of the fold. The fracture density of a single well located within the deformation adjustment zone and at the core of the fold is between $0.93\text{--}1.49 \text{ m}^{-1}$, the fracture density of a single well located only at the core of the fold is between $0.67\text{--}0.75 \text{ m}^{-1}$ and that of a single well located at the wing of the fold is between $0.35\text{--}0.59 \text{ m}^{-1}$ (Figure 9a).

5.1.3. Intrusion Promotes Local Fracture Development

Many wells in the study area encounter diabase. In the buried hill metamorphic rock mass, diabase mostly appears as thin dikes, and there are obvious anomalies in the conventional logging curves in terms of both the corresponding magnitudes and curve morphologies. Taking well BZ13-D as an example, four thin-layer diabase dike bodies were identified from shallow to deep in the buried hill. The natural gamma curve and neutron pore curve of the dike body interval are box-shaped, the density curve is funnel-

shaped, and the resistivity curve and sonic curve are finger-shaped (with low-amplitude and high-amplitude fingers, respectively). The logging values of the gamma ray curve, neutron pore curve and density curve also can be used to effectively distinguish between the diabase dike interval and the common metamorphic rock interval (Figure 12). The fracture linear density data of a single well show that the fracture linear density of the diabase dike interval and its periphery is obviously greater than that of the other intervals, which may be related to the transformation of the rock mass by intrusions. The intrusion of thin-layer diabase dikes (thickness usually less than 20–30 m) along faults increases the local stress, which not only makes the fault more open but also causes the surrounding rock to break and promotes the local development of fractures [54,55]. The intrusion of a thin diabase dike increases the heterogeneity of the rock mass, and the location of the rock layer represents the weak point of the stress. In later tectonic activities, the accumulated stress is preferentially released at the weak point of stress and its periphery, resulting in the development of many fractures in the thin diabase dike and its periphery. Although we observed this phenomenon near the intrusions in the Bozhong 13-2 area, the influence of intrusions on fracture formation at the local scale still needs further work.

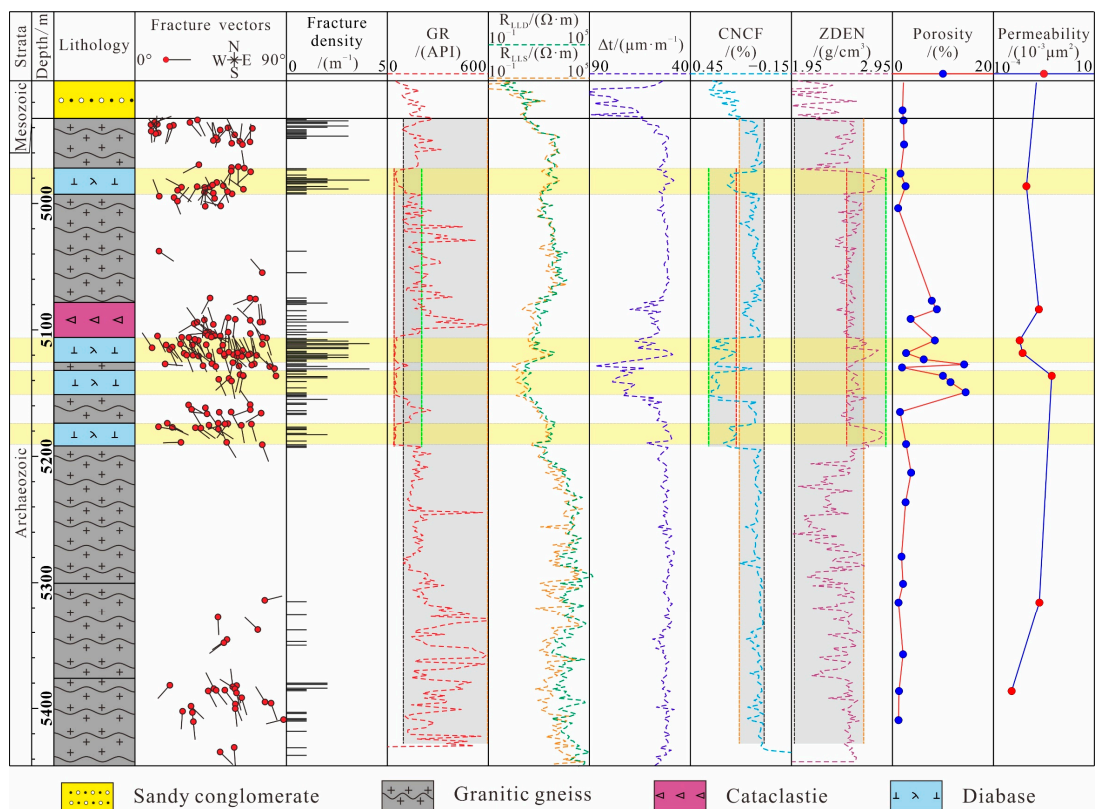


Figure 12. Stratigraphic column of well BZ13-D in Bozhong Depression, Bohai Bay Basin.

5.2. Effectiveness of Fractures and Their Influence on Reservoir Quality

5.2.1. Reactivation after Filling Ensures Fracture Effectiveness

The Archean metamorphic rocks in the Bohai Bay Basin experienced various geological events [7,28] such as structural and fluid modifications throughout geological history, forming dual-medium reservoirs composed of pores and fractures [28]. Thin section observations show that the reservoir space of the inner fracture zone of the buried hill reservoir is mainly composed of tectonic fractures and dissolution pores. The currently effective tectonic fractures were modified by previous fractures, often exhibiting reactivation including reopening after filling by further modification or dissolution of later structures. Dissolution pores often developed in minerals around the reactivated tectonic fractures, and the dissolved minerals are mainly feldspar and biotite minerals (Figure 13d). The

dissolution pores in feldspar crystals can be observed in the area of intense dissolution (Figure 13e) and partial dissolution of biotite can be observed (Figure 13a). In addition, microscopic observation revealed that the fractures in the study area underwent various diagenetic episodes after formation and the fractures were filled with various diagenetic minerals, such as calcareous, siliceous, iron and argillaceous materials (Figure 13b,f,g,h) [15] which resulted in considerable filling of tectonic fractures on a large scale from the early Indosinian to Yanshanian period. These diagenetic minerals filled the Bohai Bay Basin under an extensional tectonic background during the middle Yanshanian period [56,57]. However, thin section observation and well logging data show that most of the current effective fractures were formed by late tectonic processes and reactivation, and only a small number of unmodified effective fractures formed (Figure 13a). The reactivated fractures exhibited microscopic openings along the edge of earlier-filled fractures or partial dissolution of prefilled materials (Figure 13c,d,g). The reactivation of fractures was related to the strong dextral strike-slip action in the Bohai Bay Basin in the late Yanshanian period, during which some tectonic fractures trending N–S were produced [7,31,32]. However, the most important tectonic significance of this period lies in the reactivation and opening of massive tectonic fractures that formed from the Indosinian to the early Yanshanian period, ensuring the effectiveness of the present fractures.

5.2.2. Fractures Provide Fluid Transport Channels

As mentioned above, the reservoirs in the inner fracture zone of buried hills are classified as fracture-porosity fractures, and the reservoir space types of high-quality reservoirs mainly include fractures and dissolution pores related to fractures [7,8]. The formation of dissolution pores can be affected by fluids from various sources [8,31,32]. Previous studies have shown that deep CO₂-bearing fluids are active in the Bohai Bay Basin near basement faults [58,59] and that CO₂-bearing fluid has a significant dissolution effect on reservoirs. These fluids arrive at the reservoir from depth along a basement fault and then enter the reservoir along microfractures and result in massive dissolution of easily soluble minerals such as feldspar and biotite, expanding dissolution from the fracture edge. The dissolution pores around the fracture can be observed in thin sections, and the same phenomenon can be observed in imaging logs (Figure 6a). Dissolution along fractures greatly improves the effectiveness of fractures and the reservoir capacity [7,12]. The drilling results reveal that there is an obvious positive correlation between the porosity and permeability of the fractured zone (Figure 12), indicating that the fractures act as good fluid migration channels for dissolution. In addition, residual asphaltic materials and hydrocarbon inclusions in fractures within quartz crystals were observed in this study, indicating that fractures provide channels for hydrocarbon migration (Figure 14).

5.2.3. Fractures Provide Reservoir Space and Facilitate Hydrocarbon Accumulation

Previous studies have shown that fractures can greatly improve the quality of tight reservoirs, and the presence of fractures can increase rock porosity by approximately 15% and permeability by two–three orders of magnitude [14]. According to the relationship between porosity and permeability, as well as the relationship between pore and fracture types, reservoirs can be divided into three types (Figure 15). The first type of reservoir is a porous reservoir, where the reservoir space is dominated by dissolution pores. In this study, the proportion of porous reservoir samples is low. The second type of reservoir is a porous and fractured reservoir, where the reservoir space is dominated by dissolution pores and structural fractures. In this study, the porous and fractured reservoir samples account for a moderate proportion of the total (Figures 11a,d,e and 15). The third type of reservoir is a fracture reservoir, where the reservoir space is structural fractures (Figures 11b,e,g and 15). These reservoir samples account for the largest proportion of the total. In general, the main reservoir types are porous and fractured reservoirs. The relationship between porosity and permeability shows that the presence of fractures plays a certain role in improving the porosity of reservoirs, but the more crucial influence on reservoirs is clearly the effec-

tive improvement in reservoir permeability [60–63]. The success of the development of reservoirs is closely related to the reservoir fracture characteristics [64–67].

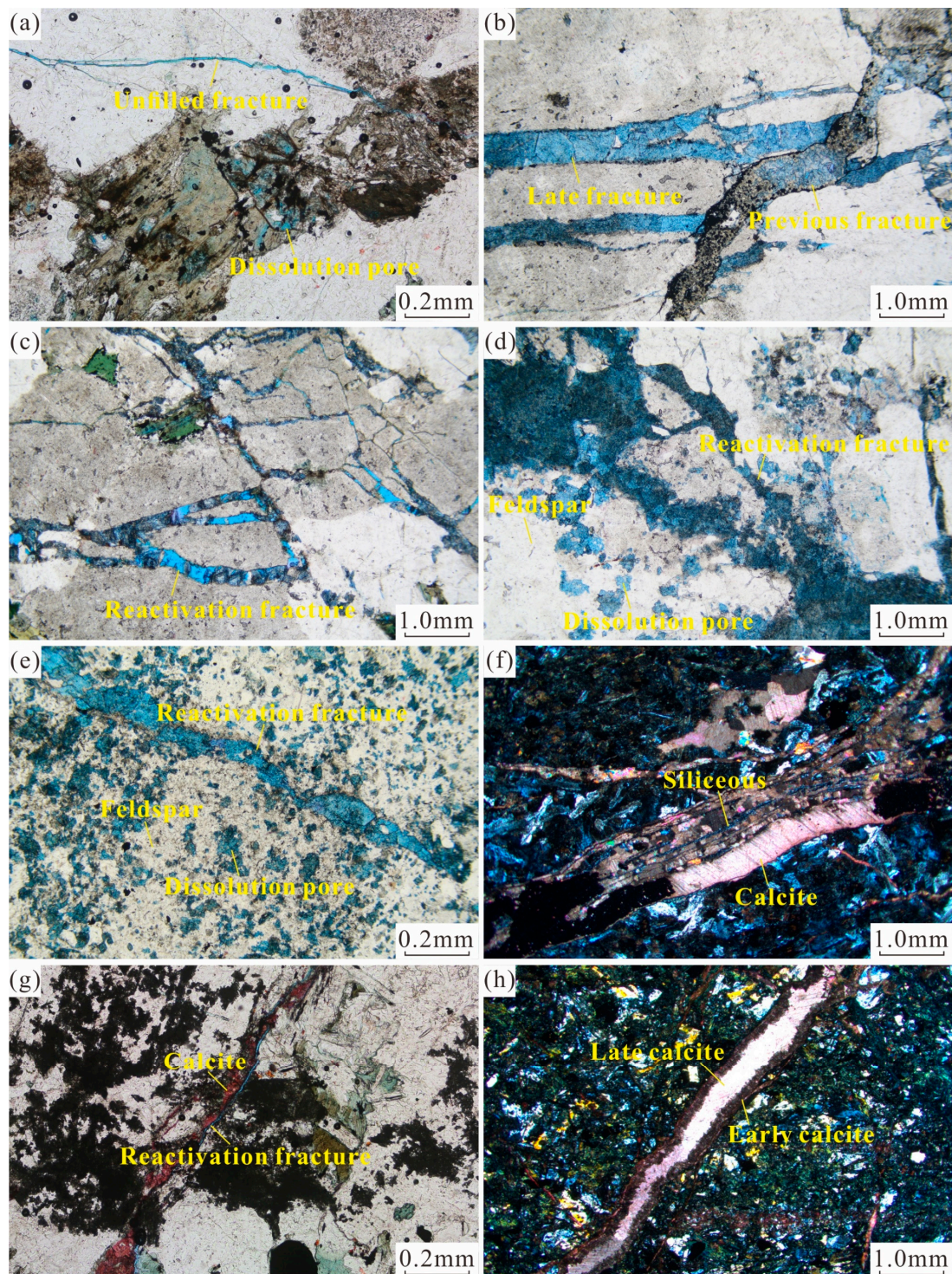


Figure 13. Fracture filling and reactivation characteristics in the inner zone of Archaeon buried hill in Bozhong 13-2 block. (a) Unfilled fractures, BZ13-E, 4690.50 m; (b) multiple stages of fractures, BZ13-B, 4686.00 m; (c) reactivation fractures, BZ13-B, 4663.00 m; (d) dissolution pore around the reactivation fracture, BZ13-B, 4744.00 m; (e) dissolution pore around the reactivation fracture, BZ13-B, 5124.00 m; (f) multiple stages filling, BZ13-D, 5122.00 m; (g) fracture filling and reactivation, BZ13-D, 5408.00 m; (h) multiple stages filling, BZ13-D, 5189.00 m.

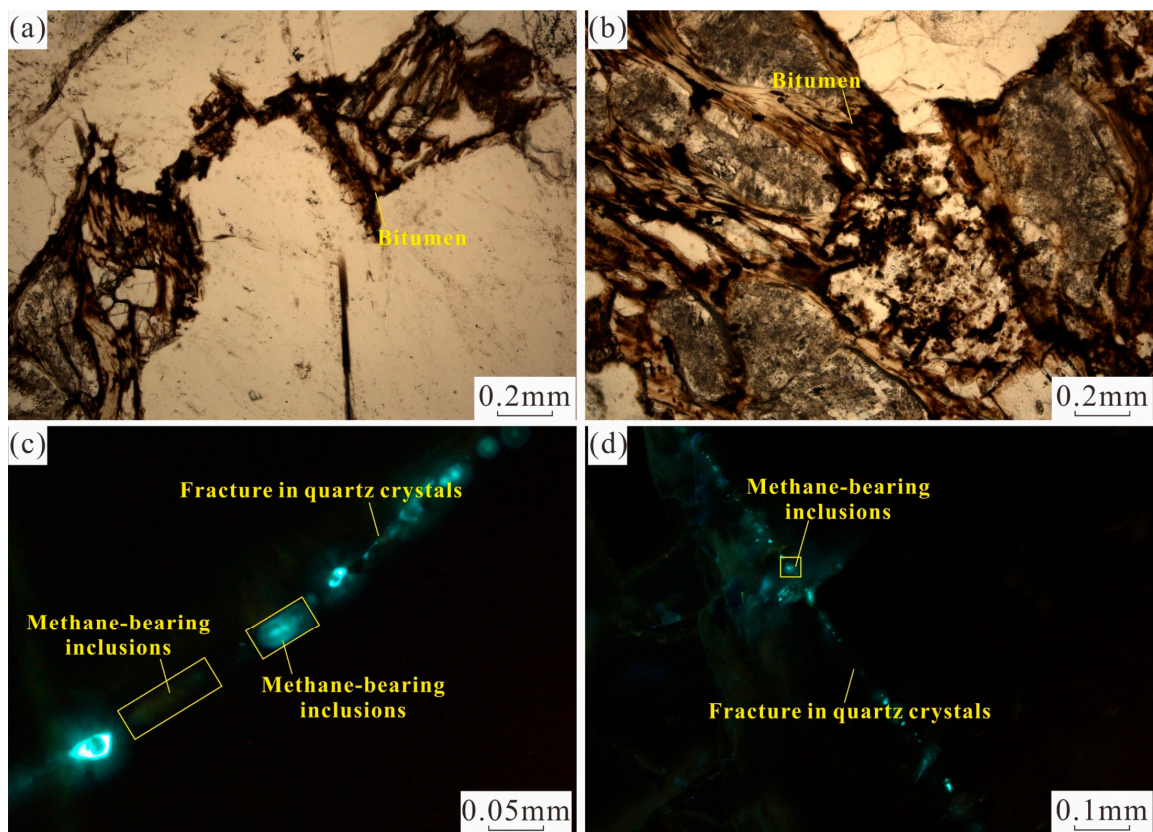


Figure 14. Bitumen and hydrocarbon inclusion characteristics in fractures in the inner zone of Archaean buried hill in Bozhong 13-2 block. (a,b) Brown diluted oil bitumen remaining in fractures, BZ13-C, 4621.00 m; (c) fluorescent hydrocarbon inclusions within quartz crystal fractures, BZ13-C, 4536.00 m; (d) fluorescent hydrocarbon inclusions within quartz crystal fractures, BZ13-C, 4717.00 m.

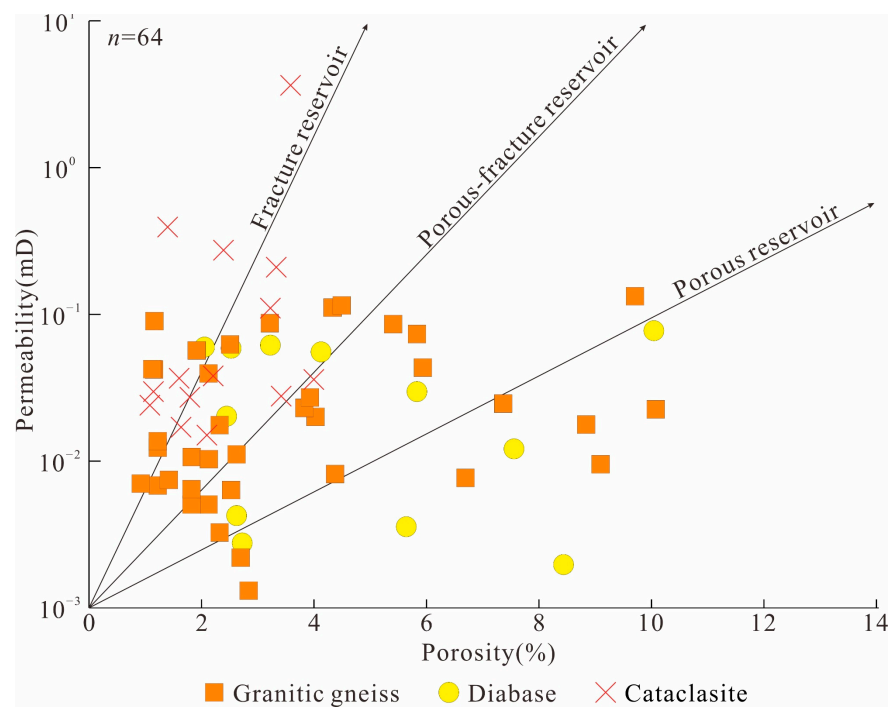


Figure 15. Reservoir types and physical properties of the inner zone of Archaean buried hill in Bozhong 13-2 block (modified after Ye et al. (2020) [60]).

Compared with sedimentary reservoirs, metamorphic reservoirs lack primary pores [68–70], and fractures have a more significant impact on the accumulation of oil and gas in the basin's crystalline basement [71–74]. We calculated the relationship between the interpretation results of oil and gas logging and the calculated fracture linear density results in each well in the study area and the fracture linear density of the oil and nonoil layers varies greatly among the wells. The fracture linear density in the oil layer of well BZ13-E reaches 2.19 m^{-1} while the fracture linear density in the oil layer of well BZ13-D is only 0.81 m^{-1} . This density is even lower than the linear fracture density in the nonoil layer of well BZ13-B (Figure 16). However, overall, the fracture density in an oil layer is obviously greater than that in a nonoil layer, which indicates that the fractures that developed in the metamorphic reservoir improve the accumulation of oil and gas.

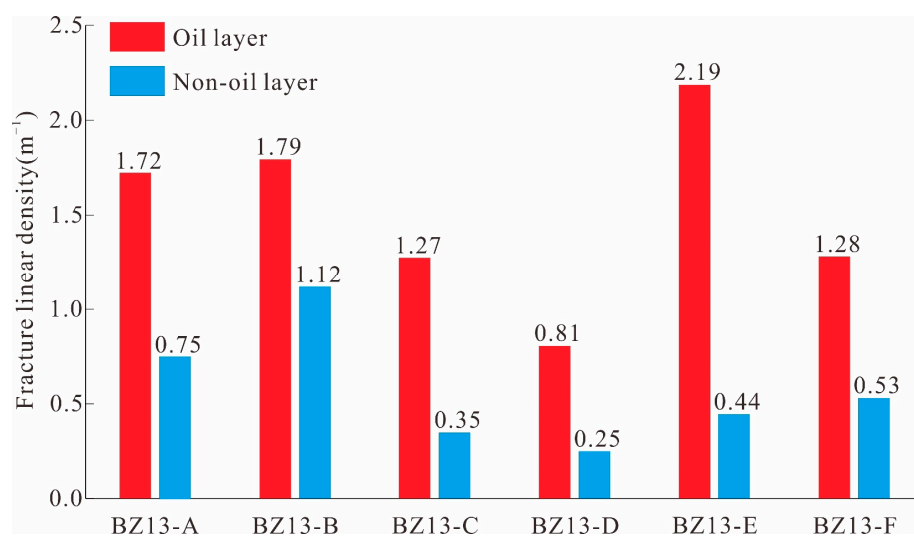


Figure 16. Fracture density in oil and nonoil zone of Bozhong 13-2 block, Bozhong Depression, Bohai Bay Basin.

6. Conclusions

- (1) Three groups of tectonic fractures are developed in the study area. The tectonic fractures striking nearly E–W, ENE and N–S were influenced by the early Indosinian thrust, late Indosinian–early Yanshanian sinistral strike-slip thrust and late Yanshanian dextral strike-slip tectonic activity, respectively, in the Bohai Bay Basin. The main formation period of the fractures ranged from the Indosinian to early Yanshanian, and late Yanshanian reactivation was the key to ensuring the effectiveness of the fractures. Imaging logging shows that 97.87% of the fractures are effective fractures. Based on thin section observation, 14.47% of the fractures are unmodified open fractures and 80.37% of the fractures are effective fractures due to reactivation.
- (2) Fractures are more developed in stress concentration areas. Laterally, the tectonic deformation adjustment zones and fold cores controlled by the thrust faults and strike-slip faults were favorable areas for fracture development. The fracture density of a single well located within the deformation adjustment zone and at the core of the fold is between $0.93\text{--}1.49 \text{ m}^{-1}$, the fracture density of a single well located only at the core of the fold is between $0.67\text{--}0.75 \text{ m}^{-1}$ and that of a single well located at the wing of the fold is between $0.35\text{--}0.59 \text{ m}^{-1}$. Vertically, the intrusion of thin diabase dikes along the faults increased local stress and promoted the development of local fractures.
- (3) The reservoir in the inner fracture zone of the buried hill is a porous-fractured and fractured reservoir. As good fluid migration channels, fractures transported fluids within the reservoir to expand the dissolution of fracture edges and promote the formation of dissolution pores. They also promoted the accumulation of oil and gas by providing reservoir space. Fractures promote the migration and accumulation of

oil and gas, and the fracture density in the oil layer is between 0.81–2.19 m⁻¹. That in the nonoil layer is between 0.25–1.12 m⁻¹.

Author Contributions: Conceptualization, J.L. and X.S.; methodology, J.L.; software, S.R., Y.S. and C.L.; validation, J.L., X.S. and J.Y.; formal analysis, J.L.; investigation, J.L.; resources, H.L. and P.X.; data curation, J.L.; writing—original draft preparation, J.L.; writing—review and editing, J.Y., A.L. and S.Y.; visualization, J.L.; supervision, X.S.; project administration, J.Y. and G.H.; funding acquisition, X.S. All authors have read and agreed to the published version of the manuscript. Authorship must be limited to those who have contributed substantially to the work reported.

Funding: National Natural Science Foundation of China (No. 41790453, No. 41972313); Major Science and Technology Special Projects of CNOOC (China) Co., Ltd. (CNOOC-KJ 135 ZDXM 36 TJ 08 TJ).

Data Availability Statement: Data available on request from the authors.

Acknowledgments: Thanks to the Tianjin Branch of CNOOC (China) Co., Ltd. for the basic data used in this project.

Conflicts of Interest: The authors declare no conflicts of interest.

References

- Luo, J.L.; Morad, S.; Liang, Z.G.; Zhu, Y.S. Controls on the quality of Archean metamorphic and Jurassic volcanic reservoir rocks from the Xinglongtai buried hill, Western depression of Liaohe basin, China. *AAPG Bull.* **2005**, *89*, 1319–1346. [[CrossRef](#)]
- Cuong, T.X.; Warren, J.K. Bach Ho field, a fractured granitic basement reservoir, Cuu Long Basin, Offshore SE Vietnam: A “buried-hill” play. *J. Pet. Geol.* **2009**, *32*, 129–156. [[CrossRef](#)]
- Dou, L.R.; Wei, X.D.; Wang, J.C.; Li, J.L.; Wang, R.C.; Zhang, S.H. Characteristics of granitic basement rock buried-hill reservoir in Bongor Basin, Chad. *Acta Pet. Sin.* **2015**, *36*, 897–904+925. [[CrossRef](#)]
- Li, W.; Dou, L.R.; Wen, Z.G.; Zhang, G.Y.; Cheng, D.S.; Hu, Y. Buried-hill hydrocarbon genesis and accumulation process in Bongor Basin, Chad. *Acta Pet. Sin.* **2017**, *38*, 1253–1262. [[CrossRef](#)]
- Nelson, R.A.; Moldovanyi, E.P.; Matcek, C.C.; Azpirixaga, I.; Bueno, E. Production characteristics of the fractured reservoirs of the La Paz Field, Maracaibo basin, Venezuela. *AAPG Bull.* **2000**, *84*, 1791–1809. [[CrossRef](#)]
- Han, C.C.; Tian, J.J.; Hu, C.L.; Liu, H.L.; Wang, W.F.; Huan, Z.P.; Feng, S. Lithofacies characteristics and their controlling effects on reservoirs in buried hills of metamorphic rocks: A case study of late paleozoic units in the Arysium depression, South Turgay basin, Kazakhstan. *J. Pet. Sci. Eng.* **2020**, *191*, 107137. [[CrossRef](#)]
- Liu, C.Y.; Li, H.Y.; Shan, X.L.; Yi, J.; Xu, P.; Ren, S.Y.; Niu, P.H. Development mechanism of metamorphic fractured reservoirs in the Bozhong area, Bohai Bay Basin: Implications from tectonic and magmatic hydrothermal activities. *Geoenergy Sci. Eng.* **2023**, *229*, 212030. [[CrossRef](#)]
- Wang, W.; Yi, J.; Shan, X.L.; Zhang, X.T.; Liu, X.J.; Liu, P.C.; Ren, S.Y. Characteristics of fractures development and its controlling factors within the buried hill reservoirs from the Archean metamorphic basement in the Bozhong Sag, Bohai Bay Basin, Eastern China. *Front. Earth Sci.* **2022**, *10*, 935508. [[CrossRef](#)]
- Ameen, M.S.; Buhidma, I.M.; Rahim, Z. The function of fractures and in-situ stresses in the Khuff reservoir performance, onshore fields, Saudi Arabia. *AAPG Bull.* **2010**, *94*, 27–60. [[CrossRef](#)]
- Liu, G.P.; Zeng, L.B.; Li, H.N.; Ostadhassan, M.; Rabiei, M. Natural fractures in metamorphic basement reservoirs in the Liaohe Basin, China. *Mar. Pet. Geol.* **2020**, *119*, 104479. [[CrossRef](#)]
- Ni, J.L.; Guo, Y.; Wang, Z.M.; Liu, J.L.; Lin, Y.X.; Li, Y. Tectonics and mechanisms of uplift in the central uplift belt of the Huimin depression. *J. Earth Sci.* **2011**, *22*, 299–315. [[CrossRef](#)]
- Tong, K.J.; Zhao, C.M.; Lv, Z.B.; Zhang, Y.C.; Zheng, H.; Xu, S.N.; Wang, J.L.; Pan, L.L. Reservoir evaluation and fracture characterization of the metamorphic buried hill reservoir in Bohai Bay. *Pet. Explor. Dev.* **2012**, *39*, 56–63. [[CrossRef](#)]
- Ju, W.; Sun, W.F. Tectonic fractures in the Lower Cretaceous Xigou Formation of Qingxi Oilfield, Jiuxi Basin, NW China Part one: Characteristics and controlling factors. *J. Pet. Sci. Eng.* **2016**, *146*, 617–625. [[CrossRef](#)]
- Ye, T.; Chen, A.Q.; Niu, C.M.; Wang, Q.B.; Hou, M.C. Characteristics, controlling factors and petroleum geologic significance of fractures in the Archean crystalline basement rocks: A case study of the South Jinzhou oilfield in Liaodong Bay depression, North China. *J. Pet. Sci. Eng.* **2022**, *208*, 109504. [[CrossRef](#)]
- Zhou, X.H.; Wang, Q.B.; Feng, C.; Ye, T.; Liu, X.J.; Hao, Y.W.; Zhou, L. Formation Conditions and Geological Significance of Large Archean Buried Hill Reservoirs in Bohai Sea. *Earth Sci.* **2022**, *47*, 1534–1548.
- Liao, X.W.; Xie, R.C.; Zhou, W.; Wang, Y.; Liu, W.C.; Liu, W.L.; Cheng, Q.; Xiong, X.J.; Luo, Z.W. The effects of paleogeomorphology on the development of fractures in reservoirs of weathering metamorphic zone in an exposed Archean burial hill, Block B, Bohai Bay Basin. *Oil Gas Geol.* **2023**, *44*, 406–417.
- Xia, L.; Zhao, Y.W.; Yu, C.L.; Xi, K.L.; Ablimiti, Y.M.; Liu, H.L.; Chen, L. Key factors controlling deep Carboniferous volcanic reservoirs in the east slope of Mahu Sag, Junggar Basin, NW China. *J. Pet. Sci. Eng.* **2023**, *220*, 111223. [[CrossRef](#)]

18. Hou, M.C.; Cao, H.Y.; Li, H.Y.; Chen, A.Q.; Wei, A.J.; Chen, Y.; Wang, Y.C.; Zhou, X.W.; Ye, T. Characteristics and controlling factors of deep buried-hill reservoirs in the BZ19-6 structural belt, Bohai sea area. *Nat. Gas Ind. B* **2019**, *39*, 33–44. [[CrossRef](#)]
19. Xu, C.G.; Du, X.F.; Liu, X.J.; Xu, W.; Hao, Y.W. Formation mechanism of high-quality deep buried-hill reservoir of Archean metamorphic rocks and its significance in petroleum exploration in Bohai Sea area. *Oil Gas Geol.* **2020**, *41*, 235–247+294.
20. Li, S.Z.; Suo, Y.H.; Santosh, M.; Dai, L.M.; Liu, X.; Yu, S.; Zhao, S.J.; Jin, C. Mesozoic to cenozoic intracontinental deformation and dynamics of the North China craton. *Geol. J.* **2013**, *48*, 543–560. [[CrossRef](#)]
21. Liu, L.; Chen, H.D.; Wang, J.; Zhong, Y.J.; Du, X.F.; Gan, X.; Zou, H. Geomorphological evolution and sediment dispersal processes in strike-slip and extensional composite basins: A case study in the Liaodong Bay Depression, Bohai Bay Basin, China. *Mar. Petroleum Geol.* **2019**, *110*, 73–90. [[CrossRef](#)]
22. Fu, Q.; You, Y.C.; Wu, Z. Tectonic episodes and reservoir fissure systems in Caotai metamorphic buried hill reservoir. *Pet. Explor. Dev.* **2003**, *30*, 18–20.
23. Zhou, X.H.; Xiang, H.; Yu, S.; Wang, G.; Yao, C.H. Reservoir characteristics and development controlling factors of JZS Neo-Archean metamorphic buried hill oil pool in Bohai Sea. *Pet. Explor. Dev.* **2005**, *32*, 17–20.
24. Wang, Y.G.; Geng, B.; Zhang, D.J. Reservoir characteristics and logging interpretation of Chengbei metamorphic rock in Jiyang depression. *Pet. Geol. Recovery Effic.* **2013**, *20*, 48–51+114.
25. Xue, Y.A. The breakthrough of the deep-buried gas exploration in the Bohai Sea area and its enlightenment. *Nat. Gas Ind.* **2019**, *39*, 11–20.
26. Li, H.Y.; Niu, C.M.; Xu, P.; Liu, Q.S.; Zhang, X.; Cui, H.Z. Discovery of Bozhong 13-2 Archean large monoblock volatile buried hill oilfield and its oil and gas exploration significance. *Nat. Gas Ind.* **2021**, *41*, 19–26. [[CrossRef](#)]
27. Yi, J.; Li, H.Y.; Shan, X.L.; Hao, G.L.; Yang, H.F.; Wang, Q.B.; Xu, P.; Ren, S.Y. Division and identification of vertical reservoir units in Archeozoic metamorphic buried hill of Bozhong Sag, Bohai Bay Basin, East China. *Pet. Explor. Dev.* **2022**, *49*, 1282–1294. [[CrossRef](#)]
28. Du, X.F.; Liu, X.J.; Zhang, X.T.; Liu, Y.J.; Xu, Y.H. Characteristics and controlling factors of Archean metamorphic reservoirs in Bohai sea area. *China Offshore Oil Gas* **2021**, *33*, 15–27.
29. Jiang, Y.L.; Ye, T.; Zhang, S.W.; Liu, H. Enrichment characteristics and main controlling factors of hydrocarbon in buried hill of Bohai Bay Basin. *J. China Univ. Pet. Ed. Nat. Sci.* **2015**, *39*, 20–29.
30. Xue, Y.A.; Wang, Q.; Niu, C.M.; Miao, Q.Y.; Liu, M.X.; Yin, J. Hydrocarbon charging and accumulation of BZ 19-6 gas condensate field in deep buried hills of Bozhong Depression, Bohai Sea. *Oil Gas Geol.* **2020**, *41*, 891–902.
31. Xiao, S.G.; Lv, D.Y.; Hou, M.C.; Hu, H.W.; Huang, Z. Mesozoic tectonic evolution and buried hill formation mechanism in the southwestern Bohai Sea. *Nat. Gas Ind.* **2019**, *39*, 34–44.
32. Zhou, Q.J.; Liu, Y.J.; Wang, D.Y.; Guan, Q.B.; Wang, G.Z.; Wang, Y.; Li, Z.T.; Li, S.Z. Mesozoic Cenozoic tectonic evolution and buried hill formation in central Bohai Bay. *Earth Sci. Front.* **2022**, *29*, 147–160. [[CrossRef](#)]
33. Xue, Y.A.; Li, H.Y.; Xu, P.; Liu, Q.S.; Cui, H.Z. Recognition of oil and gas accumulation of Mesozoic covered buried hills in Bohai sea area and the discovery of BZ13-2 oilfield. *China Offshore Oil Gas* **2021**, *33*, 13–22.
34. Lai, J.; Li, D.; Wang, G.W.; Xiao, C.W.; Hao, X.L.; Luo, Q.Y.; Lai, L.B.; Qin, Z.Q. Earth stress and reservoir quality evaluation in high and steep structure: The Lower Cretaceous in the Kuqa Depression, Tarim Basin, China. *Mar. Pet. Geol.* **2019**, *101*, 43–54. [[CrossRef](#)]
35. Liu, Z.Q.; Shi, B.B.; Ge, T.C.; Sui, F.G.; Wang, Y.; Zhang, P.F.; Chang, X.C.; Liu, Y.; Wang, Y.R.; Wang, Z.Y. Tight sandstone reservoir sensitivity and damage mechanism analysis: A case study from Ordos Basin, China and implications for reservoir damage prevention. *Energy Geosci.* **2022**, *3*, 394–416. [[CrossRef](#)]
36. Aydin, A. Fractures, faults, and hydrocarbon entrapment, migration and flow. *Mar. Pet. Geol.* **2000**, *17*, 797–814. [[CrossRef](#)]
37. Islamov, S.; Islamov, R.; Shelukhov, G.; Sharifov, A.; Sultanbekov, R.; Ismakov, R.; Agliullin, A.; Ganiev, R. Fluid-Loss Control Technology: From Laboratory to Well Field. *Processes* **2024**, *12*, 114. [[CrossRef](#)]
38. Thang, N.V.; Vinh, P.T.; Rogachev, M.K.; Korobov, G.Y.; Parfenov, D.V.; Zhurkevich, A.O.; Islamov, S.R. A comprehensive method for determining the dewaxing interval period in gas lift wells. *J. Pet. Explor. Prod. Technol.* **2023**, *13*, 1163–1179. [[CrossRef](#)]
39. Awdal, A.; Healy, D.; Alsop, G.I. Fracture patterns and petrophysical properties of carbonates undergoing regional folding: A case study from Kurdistan, N Iraq. *Mar. Pet. Geol.* **2016**, *71*, 149–167. [[CrossRef](#)]
40. Keeton, G.I.; Pranter, M.J.; Cole, R.D.; Gustason, E.R. Stratigraphic architecture of fluvial deposits from borehole images, spectral-gamma-ray response, and outcrop analogs, Piceance Basin, Colorado. *AAPG Bull.* **2015**, *99*, 1929–1956. [[CrossRef](#)]
41. Van Golf-Racht, T.D. *Fundamentals of Fractured Reservoir Engineering*; Elsevier Scientific Publishing Company: New York, NY, USA, 1989; p. 710.
42. Ding, W.L.; Zhu, D.W.; Cai, J.J.; Gong, M.L.; Chen, F.Y. Analysis of the developmental characteristics and major regulating factors of fractures in marine–continental transitional shale–gas reservoirs: A case study of the Carboniferous–Permian strata in the southeastern Ordos Basin, central China. *Mar. Pet. Geol.* **2013**, *45*, 121–133. [[CrossRef](#)]
43. Zheng, H.; Kang, K.; Liu, W.L.; Gong, M.; Chen, S.B. Main controlling factors and prediction of fractures in deep metamorphic buried hill reservoirs in Bohai Sea. *Lithol. Reserv.* **2022**, *34*, 29–38.
44. Wang, Y.; Xu, C.Q.; Guo, L.L.; Liu, Y.J.; Wang, G.Z.; Liu, B.; Li, S.Z.; Guan, Q.B.; Jiang, L.W.; Chen, Z.X.; et al. Structural Analysis of Shijiutuo East 428 Buried Hill in Bohai Bay Basin: Implications on Destruction of the North China Craton. *Geotecton. Metallog.* **2021**, *45*, 219–228.

45. Qi, J.F.; Yu, F.S.; Lu, K.Z.; Zhou, J.X.; Wang, Z.Y.; Yang, Q. Conspectus on Mesozoic basins in Bohai Bay province. *Earth Sci. Front.* **2003**, *10*, 199–206.
46. Wang, R.Y.; Ding, W.L.; Zhang, Y.Q.; Wang, Z.; Wang, X.H.; He, J.H.; Zeng, W.T.; Dai, P. Analysis of developmental characteristics and dominant factors of fractures in Lower Cambrian marine shale reservoirs: A case study of Niutitang formation in Cen'gong block, southern China. *J. Pet. Sci. Eng.* **2016**, *138*, 31–49. [[CrossRef](#)]
47. Luan, H.; Cao, Y.; Jiang, Y.; Guan, Y.; Li, C.; Zhang, S.; Liu, J. Implementation of tension-shear coupling failure mode of rock bolts in FLAC3D and its application. *J. Min. Strat. Control Eng.* **2022**, *4*, 063029. [[CrossRef](#)]
48. Zhao, G.; Ding, W.L.; Sun, Y.X.; Wang, X.H.; Tian, L.; Liu, J.S.; Shi, S.Y.; Jiao, B.C.; Cui, L. Fracture development characteristics and controlling factors for res-ervoirs in the Lower Silurian Longmaxi Formation marine shale of the Sangzhi block, Hunan Province, China. *J. Pet. Sci. Eng.* **2020**, *184*, 106470. [[CrossRef](#)]
49. Osinowo, O.; Abdulmumin, Y.; Faweya, T. Analysis of high-resolution airborne-magnetic data for hydrocarbon generation and preservation potential evaluation of Yola sub-basins, northern Benue Trough, northeastern Nigeria. *Energy Geosci.* **2023**, *4*, 33–41. [[CrossRef](#)]
50. Li, R.Q.; Lv, W.Y.; Wang, H.N.; Li, J.; Liu, Y.L.; Yuan, J. Distribution characteristics of natural fractures of the typical fault anticlines in Keshen area of Kelasu Structural Belt, Kuqa Depression, Tarim Basin. *Nat. Gas Geosci.* **2023**, *34*, 271–284.
51. Yin, S.; Wu, Z. Geomechanical simulation of low-order fracture of tight sandstone. *Mar. Pet. Geol.* **2020**, *100*, 1–10. [[CrossRef](#)]
52. Liu, Z.Y. Research on Fracture Initiation and Expansion Law of Fractured Fracture in Fractured Reservoirs by Acer's Finite-discrete Element Method. Ph.D. Thesis, Northeast Petroleum University, Daqing, China, 2022; pp. 43–46.
53. Yin, S.; Dong, L.; Yang, X.; Wang, R. Experimental investigation of the petrophysical properties, minerals, elements and pore structures in tight sandstones. *J. Nat. Gas Sci. Eng.* **2020**, *76*, 1–14. [[CrossRef](#)]
54. Bate, B.B.; Boboye, O.A.; Fozao, K.F.; Ndip, E.A.; Anene, N.O. Petrophysical characterization and 3D seismic interpretation of reservoirs in the Baris Field, onshore Niger Delta Basin, Nigeria. *Energy Geosci.* **2023**, *4*, 103–116. [[CrossRef](#)]
55. Yin, S.; Han, C.; Wu, Z.; Li, Q. Developmental characteristics, influencing factors and prediction of fractures for a tight gas sandstone in a gentle structural area of the Ordos Basin, China. *J. Nat. Gas Sci. Eng.* **2019**, *72*, 1–14. [[CrossRef](#)]
56. Yin, X.Y.; Liu, X.X.; Cao, D.P. Elastic parameters calculation for tight sand reservoir based on Biot-consistent theory. *Geophys. Prospect. Pet.* **2013**, *52*, 445–450.
57. Zhang, S.; Wang, L.; Yang, H.; Lu, L. Construction and numerical simulation research of functional supporting in deep roadways. *J. Min. Strat. Control Eng.* **2023**, *5*, 013012. [[CrossRef](#)]
58. Zhou, X.H.; Zhang, C.R.; Li, H.Y.; Wang, B.Q.; Guo, Y.H. Major controls on natural gas accumulations in deep-buried hills in Bozhong Depression, Bohai Bay Basin. *J. China Univ. Pet. (Ed. Nat. Sci.)* **2017**, *41*, 42–50.
59. Zhou, X.; Sun, L. Factors controlling the formation and evolution of source rocks in the Shahezi Formation, Xujiaweizi fault depression, Songliao Basin. *Energy Geosci.* **2023**, *4*, 100140. [[CrossRef](#)]
60. Ye, T.; Niu, C.M.; Wei, A.J. Characteristics and genetic mechanism of large granitic buried-hill reservoir, a case study from PengLai oil field of Bohai Bay Basin, north China. *J. Pet. Sci. Eng.* **2020**, *189*, 106988. [[CrossRef](#)]
61. Wang, Z.; Zhang, K.; Cheng, Y.; Wu, Q. Identification and evaluation of fault-fracture reservoirs in buried hills of the Lower Paleozoic, Chengdao area, China. *Energy Geosci.* **2023**, *4*, 100183. [[CrossRef](#)]
62. Wu, Z.; Cui, C.; Jia, P.; Wang, Z.; Sui, Y. Advances and challenges in hydraulic fracturing of tight reservoirs: A critical review. *Energy Geosci.* **2022**, *3*, 427–435. [[CrossRef](#)]
63. Zhu, L.; Gu, W.; Chai, J.; Ma, Z.; Qiu, F. Evolution of mining-induced overburden deformation using distributed optical fiber. *J. Min. Strat. Control Eng.* **2022**, *4*, 013014. [[CrossRef](#)]
64. Zhou, H.Y.; Zhao, C.M.; Yin, Z.J. Development and distribution of the metamorphite-weathering crust and its feature of reservoir-property for the JZS buried Hill, Liaodongwan area. *Nat. Gas Geosci.* **2015**, *26*, 599–607.
65. Liu, J.L.; Liu, Z.Q.; Liu, Z.F.; Liu, Y.L.; Shen, B.J.; Xiao, K.H.; Bi, Y.Y.; Wang, X.W.; Wang, A.; Fan, L.X.; et al. Geological characteristics and models of fault-fold-fracture body in deep tight sandstone of the second member of Upper Triassic Xujiahe Formation in Xinchang structural belt of Sichuan Basin, SW China. *Pet. Explor. Dev.* **2023**, *50*, 603–614. [[CrossRef](#)]
66. Zhu, L.; Zhou, X.; Liu, W.; Kong, Z. Total organic carbon content logging prediction based on machine learning: A brief review. *Energy Geosci.* **2023**, *4*, 100098. [[CrossRef](#)]
67. Zhu, Q.; Dai, J.; Yun, F.; Zhai, H.; Zhang, M.; Feng, L. Dynamic response and fracture characteristics of granite under microwave irradiation. *J. Min. Strat. Control Eng.* **2022**, *4*, 019921. [[CrossRef](#)]
68. Nan, Z.; Fu, W.; Liu, Z. Numerical simulation and response analysis of microspherical focused logging in inclined micro-fractured formation. *Energy Geosci.* **2023**, *4*, 100063. [[CrossRef](#)]
69. Wang, K.; Liu, H.C.; Ren, W.W.; Li, W.Q.; Yu, Z.Q. Influence of Cenozoic Diabase Intrusion on Reservoir Properties of Mudstone Wallrocks in the Yangxin Sub-depression, Subei Basin. *Geoscience* **2022**, *36*, 1563–1573.
70. Wang, D.Y.; Liu, X.J.; Deng, H.; Liu, Y.J.; Li, D.Y. Characteristics of the Meso-Cenozoic tectonic transformation and its control on the formation of large scale reservoirs in the Archean buried hills in Bozhong 19-6 area, Bohai Bay Basin. *Oil Gas Geol.* **2022**, *43*, 1334–1346.
71. Ji, B.; Fang, J. An overview of efficient development practices at low permeability sandstone reservoirs in China. *Energy Geosci.* **2023**, *4*, 100179. [[CrossRef](#)]

72. Zhang, P.; Xu, D.; Fu, X.; Xie, J.; Dong, Y.; Zhang, X. Evaluation of hydraulic conductivity based on fault confinement studies. *J. Min. Strat. Control Eng.* **2022**, *4*, 023033. [[CrossRef](#)]
73. Ge, X.; Myers, M.; Li, J. Recent advances in petrophysical and geophysical characterization of unconventional resources: Introduction. *Energy Geosci* **2023**, *4*, 100120. [[CrossRef](#)]
74. Khan, A.; Gul, M.; Awan, R.; Khan, A.; Iltaf, K.; Butt, S. 2D seismic interpretation of Sawan gas field integrated with petrophysical analysis: A case study from Lower Indus Basin, Pakistan. *Energy Geosci.* **2023**, *4*, 100143. [[CrossRef](#)]

Disclaimer/Publisher's Note: The statements, opinions and data contained in all publications are solely those of the individual author(s) and contributor(s) and not of MDPI and/or the editor(s). MDPI and/or the editor(s) disclaim responsibility for any injury to people or property resulting from any ideas, methods, instructions or products referred to in the content.